

Cite this: *Chem. Soc. Rev.*, 2012, **41**, 7938–7961

www.rsc.org/csr

CRITICAL REVIEW**Defect-related luminescent materials: synthesis, emission properties and applications****Cuimiao Zhang^{ab} and Jun Lin^{*a}***Received 25th March 2012*

DOI: 10.1039/c2cs35215j

Luminescent materials have found a wide variety of applications, including information displays, lighting, X-ray intensification and scintillation, and so on. Therefore, much effort has been devoted to exploring novel luminescent materials so far. In the past decade, defect-related luminescent materials have inspired intensive research efforts in their own right. This kind of luminescent material can be basically classified into silica-based materials, phosphate systems, metal oxides, BCNO phosphors, and carbon-based materials. These materials combine several favourable attributes of traditional commercially available phosphors, which are stable, efficient, and less toxic, being free of the burdens of intrinsic toxicity or elemental scarcity and the need for stringent, intricate, tedious, costly, or inefficient preparation steps. Defect-related luminescent materials can be produced inexpensively and on a large scale by many approaches, such as sol–gel process, hydro(solvothermal) reaction, hydrolysis methods, and electrochemical methods. This review article highlights the recent advances in the chemical synthesis and luminescent properties of the defect-related materials, together with their control and tuning, and emission mechanisms (solid state physics). We also speculate on their future and discuss potential developments for their applications in lighting and biomedical fields.

1. Introduction

Luminescent materials (or phosphors) are generally characterized by the emission of light in the visible range but can also be in other spectral regions (such as ultraviolet or infrared) with energy beyond thermal equilibrium.^{1,2} The ever-growing demand for advanced luminescent materials has motivated scientific and

^a State Key Laboratory of Rare Earth Resources Utilization, Changchun Institute of Applied Chemistry, Chinese Academy of Sciences, Changchun 130022, P. R. China. E-mail: jlin@ciac.jl.cn; Fax: (+86) 431-85698041

^b College of Chemistry and Environmental Science, Hebei University, Baoding 071002, P. R. China. E-mail: cuimiaozhang@yahoo.cn

**Cuimiao Zhang**

Cuimiao Zhang was born in Hebei, China, in 1980. She received her BS (2004) in chemistry from Hebei University. Then she has been a graduate student in Jun Lin's group at Changchun Institute of Applied Chemistry (CIAC), Chinese Academy of Sciences, and received a PhD degree in 2010. After graduation, she has been working as a research fellow in Nanyang Technological University (Singapore, 2010–2012). Her current research interests include the synthesis of environmentally-friendly luminescence materials and their bioapplication. She came back to China in 2012, and since then has been working as an assistant professor in Hebei University.

**Jun Lin**

Jun Lin was born in Changchun, China, in 1966. He received BS and MS degrees in inorganic chemistry from Jilin University, China, in 1989 and 1992, respectively, and a PhD degree (inorganic chemistry) from the Changchun Institute of Applied Chemistry (CIAC), Chinese Academy of Sciences, in 1995. Then he went to CityU (HK, 1996), INM (Germany, 1997), VCU and UNO (USA, 1998–1999) working as a postdoctor. He came back to China in 2000, and since then has been working as a professor in CIAC. His research interests include luminescent materials and multifunctional composite materials together with their applications in display, lighting and biomedical fields.

technological efforts dedicated to improving existing phosphors and to developing new effective luminescent materials.³ Generally, inorganic luminescent materials can be classified into two groups: metal-activator based and non-activator based luminescent materials. The first case is represented by transitions between energy levels of metal activator ions containing the rare earth and/or transition metal ions (*e.g.* f-f transitions of Eu³⁺ in Y₂O₃:Eu³⁺)^{4–7} or complex ions (*e.g.* the charge-transfer transition on [WO₄]²⁻ in CaWO₄).^{8,9} These kinds of luminescent materials are often expensive and contain non-environmentally friendly elements, such as Ag (in ZnS:Ag⁺) and lanthanides.^{1–15} On the other hand, it is necessary for most metal-activator-based phosphors to be excited by short-wavelength ultraviolet (UV) light for operation, which results in the extensive use of a mercury vapor plasma in fluorescent lighting products.^{1,10} The excess usage of mercury vapor will give rise to environmental contamination and technical difficulties. The other group of luminescent materials consists of semiconductors and defect-related materials. For most semiconductors, the luminescence normally results from band-to-band excitation between impurity states within the bandgap. However, some serious intrinsic toxicity and potential environmental hazards associated with many of these semiconductors are critically pronounced, which have limited their applications. For the defect-related luminescent materials, although the roots can be traced to 1986,¹⁶ they have had a remarkable growth since Sailor *et al.* reported the white phosphors from a silicate-carboxylate sol-gel precursor.¹⁷ Since then, the emerging defect-related luminescent materials, which do not contain any transition metal or rare earth activators, appear to be promising alternatives to traditional phosphors in many applications because of their advantages of low toxicity, stability, tunable emission color, and low cost.^{17–30} Although the origins of photoluminescence (PL) are not yet entirely understood in defect-related materials, there is mounting evidence that emission arises from the special defects. Typically, the defects in these kind of materials contain vacancies, impurities, radical impurities, donor-acceptor pairs, *etc.*,^{22,27,31–33} which may arouse charge imbalances at these defect sites. The charge imbalances must be rectified by localization of electrons and electron holes or give rise to impurity states within the bandgap. Therefore, the defect sites are apparently the precursors for various centers containing the emission center for defect-related luminescent materials and impart them with excellent photoluminescent emission.

On the other hand, in modern chemistry and materials science, there have been tremendous developments in the synthetic control of size, shape, and composition, thus allowing the tailoring of their properties.^{34–40} Therefore, the synthesis methods have been intensively pursued for their technological and fundamental scientific importance.^{41,42} Among them, the luminescence properties of defect-related luminescent materials can also be influenced by their phase, surface chemistry, size distribution, morphology and/or porosity.^{43–45} Thus, the rational control over these factors has become an important research issue in recent years.⁴⁶ So far, valuable explorations have been carried out based on soft chemical synthetic strategies [such as Pechini sol-gel (PSG) method, hydrothermal process, and so on] to luminescent materials as well as controlled morphologies, formation, and luminescence properties.

As we know, the tremendous recent advances in functionalized nanomaterials with distinct fluorescent properties,^{47–54} mesoporous properties,⁵⁵ and biocompatibility^{56,57} have received considerable attention in the past decades, since nanomaterials provide a new platform for biomedical applications such as drug delivery, bio-separation, fluorescent labeling,⁵⁸ diagnosis and treatment of disease.^{59–68} During the past decades, the use of semiconductor fluorescent nanocrystals or quantum dots has notably extended the scope of possible biological applications (fluorescent probes, labeling and tracking, *etc.*) due to their high quantum yield and high photostability.^{69,70} However, their disadvantages of blinking, potential cytotoxicity *in vivo*, and complex functionalization strategies have limited their use. Additionally, some serious problems of photobleaching and quenching of fluorescent organic molecules are critically pronounced, which have seriously limited their applications in biomedical areas.^{60,71,72} In contrast to traditional fluorescent materials in biological areas such as organic dyes and quantum dots, the novel defect-related luminescent nanomaterials may be promising fluorescent materials in biological fields due to their good optical properties, high chemical stability, and low toxicity.^{29,30,73–77} Especially, multifunctional defect-related materials with excellent luminescent, structural, and/or surface properties seem to be ideal systems for biomedical applications. To date, many recent reports have shown that multifunctional defect-related materials, as the most efficient fluorescent materials, can be used for the intracellular imaging, drug delivery, and so on.^{26,29,30,78}

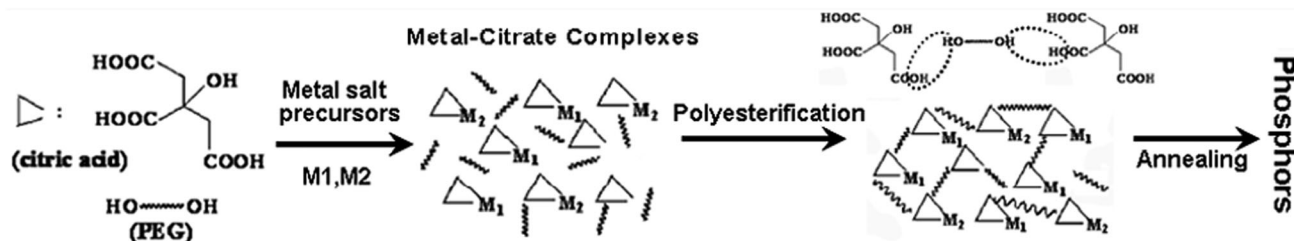
In this review article, we mainly focus on the recent progress in various chemical syntheses and luminescent properties of defect-related luminescent materials, together with their tuning and possible emission mechanisms as well as their applications in lighting, display, and biological fields (including bioimaging and tracking in drug delivery systems), based on our recent efforts and those of others in this area. Moreover, we hope to inspire research into the origins of the unique properties of this emergent class of novel luminescent materials and to encourage their exploration in a multitude of exciting areas from lighting to display and medical diagnostics.

2. Synthetic methods

Generally, as the defect sites are mainly created in the preparing process, the luminescent properties of defect-related materials seem to be dominated by the preparation methods. In recent years, a large number of synthetic methods have been developed for generating defect-related luminescent materials. These methods can be divided into several categories: sol-gel method, hydro-(solvo)thermal reaction, hydrolysis method, electrospinning process, sonochemical synthesis, chemical vapor deposition (CVD), and so on. Typically, the common features of all these methods of synthesis are the need of heat treatments (high or low temperature) and/or organic groups (surfactants, organic additives, templates, *etc.*).

2.1. Sol-gel method

Undoubtedly, the sol-gel technique is one of the most well-known soft solution processes, which can be generally divided into three types: sol-gel route based on the hydrolysis and



Scheme 1 Basic principle of Pechini sol–gel process to synthesize phosphors (reproduced with permission from ref. 79, copyright 2007, American Chemical Society).

condensation of molecular precursors, gelation route based on concentration of aqueous solutions containing metal-chelates (called “chelate gel” route), and polymerizable complex route (named Pechini-type sol–gel process).^{79–81} Commonly, silicon alkoxides, metal alkoxides, or organic additives [such as citric acid and polyethylene glycol (PEG)] are employed in the sol–gel process, following heat treatment to remove the organic groups produced by alcoholysis of alkoxides or organic additives. Interestingly, it is also possible to utilize some defects (such as carbon impurities and vacancies) as emission centers to get novel defect-related luminescent materials.^{17,79} It has been reported that sol–gel-derived SiO₂-based materials, including silica gels (xerogels or aerogels),^{28,82} porous silica,⁸³ multicomponent silica-based oxide materials,⁸⁴ silicate-carboxylate,¹⁷ and inorganic–organic hybrids,^{18,85} all show strong luminescence from the blue to red spectral region,^{17–19,27} and even ultraviolet photoluminescence.⁸³ They can potentially be used as environmentally friendly luminescent materials without expensive or toxic metal elements as activators.

Pechini-type sol–gel process (PSG), which uses common metal salts as precursors, citric acid as a chelating ligand of metal ions and polyhydroxy alcohol as a cross-linking agent to form a polymeric resin on the molecular level, can reduce segregation of particles and ensure compositional homogeneity. These advantages can overcome most of the difficulties and disadvantages that frequently occur in the alkoxide-based sol–gel process (high cost, fast hydrolysis rate, and so on). Pechini-type sol–gel method followed by heat treatment at moderate temperature can remove organic additives and generate a pure phase of multiple components (Scheme 1).⁷⁹ During this annealing process, hydrocarbon residues cannot be removed completely, which may induce carbon impurities and form other kinds of defects in the host lattice (such as the oxygen defects). It is possible to utilize these defects as emission centers to obtain novel phosphors without rare earth or transition metal ions as activators. In the past several years, our group has synthesized various kinds of highly efficient defect-related phosphors by PSG. We found that the PSG process-derived BPO₄ exhibits a weak purple-colored emission under UV irradiation caused by the carbon impurities. Doping it with alkaline earth metal and alkali metal ions^{86,87} or mixing with SiO₂ or Al₂O₃⁸⁸ produced a series of BPO₄-based materials that emit an efficient bluish-white light with a quantum yield more than 31%, which is induced by carbon impurities, peroxy radicals, and/or oxygen vacancies defects, respectively. Besides BPO₄-based phosphors, the same phenomena were also observed in Al₂O₃,⁸⁹ ZrO₂,⁴³ and silica/apatite composite⁹⁰ prepared by PSG process (Fig. 1), which

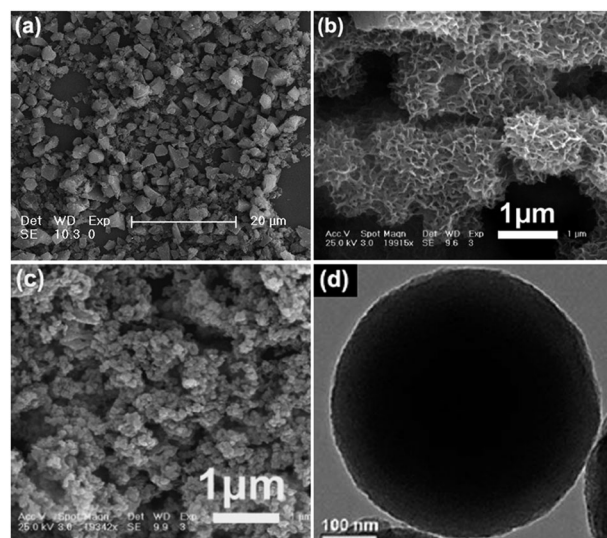


Fig. 1 Representative shapes of defect-related luminescent materials obtained by Pechini-type sol–gel process. SEM images of BPO₄:6%Li⁺ (a), Al₂O₃ (b), ZrO₂ (c) (reproduced with permission from ref. 87, 89 and 43, copyright 2009, 2008, and 2007, American Chemical Society), and silica/apatite composite (d) (reproduced with permission from ref. 90, copyright 2011, Royal Society of Chemistry).

can also show efficient, stable, and/or tunable luminescence. In addition, some titanates (CaTiO₃, SrTiO₃, and BaTiO₃) exhibiting an intense photoluminescence were also prepared by PSG method followed by calcination at 300–400 °C.^{91,92} For the sol–gel method, the annealing procedure (temperature and annealing time) is the key step in the synthesis process, which can seriously affect the types and quantities of the defects in the materials and their luminescent properties.

2.2. Hydro(solvo)thermal reaction

It is well known that the hydrothermal method is a typical solution-based method that exploits water or organic solvents under certain temperatures and pressures, and has received much attention.⁹³ Over the past decade, various micro- and/or nano-crystals, which exhibit many interesting shape- and size-dependent phenomena and properties, have been synthesized by the hydrothermal process and extensively investigated for both their scientific and technological applications.^{94–99} Especially, the water-based systems with environmentally acceptable and relatively low cost advantages provide a relatively green chemical alternative to the preparation of various inorganic materials.^{38,100–102} To date, different defect-related luminescent

materials have been successfully prepared by the simple hydrothermal method. For instance, based on the hydrothermal treatment at designated reaction conditions (such as reaction temperature and time, chelating ligands, organic additives, etc.), a systematic study has been carried out to investigate the controlled formation of a series of apatite structure micro-/nano-crystals with environmentally friendly defect-related luminescent properties.^{103–106} The general synthetic methodology for the apatite structures is shown in the top of Fig. 2. As an example, the hydroxyapatite (HAp) phosphors via hydrothermal process [trisodium citrate as chelating ligands and hexadecyltrimethylammonium bromide (CTAB) as surfactants] with narrow size distribution and novel morphologies and architectures, such as nanorods, nanowires, nanoparticles, microspheres, micro-flowers, microsheets, and microspheres (Fig. 2a–f), are of special significance in understanding the growth behavior and influence on defect-related luminescent properties.¹⁰³ Moreover, there are several important key factors for final shapes of HAp nano/microcrystals, which contains pH values, organic additive (CTAB), and trisodium citrate (Fig. 2).^{107,108} The metal-chelating trisodium citrate ligands can not only affect the morphology of the sample, but also the key factor for the defect-related luminescent properties. During the crystal growth of HAp, the trisodium citrate can slow down the nucleation and subsequent crystal growth of HAp particles and change the relative surface energy of different crystal facets, which results in the formation of different HAp structures.¹⁰⁹ On the other hand, the electron paramagnetic resonance (EPR) results indicates that the luminescent-related paramagnetic defects ($\text{CO}_2^{\bullet-}$) can be induced

by trisodium citrate during the hydrothermal process. Under the high pressure and thermal process, bond cleavages can occur in some citrate anions, which result in $\text{R}-\text{C}^{\bullet}$ and $\text{CO}_2^{\bullet-}$. Small amounts of $\text{CO}_2^{\bullet-}$ radicals resulting from the bond cleavages are trapped by the already formed hydroxyapatite lattice or interstitial positions. The residual fragmented bonds ($\text{CO}_2^{\bullet-}$) are apparently the precursors for various centers, such as luminescent centers.

Apart from the investigation of the HAp nano/microcrystals, we also utilized a similar method to synthesize other apatite structures with defect-related luminescent properties, such as calcium fluorapatite (FAP) nanorods, strontium hydroxyapatite (SrHAp) with various morphologies (nanorods and architecture microspheres). Fig. 2g–i shows the representative morphologies of FAP and SrHAp products. We found that the molar ratio of metal ions and chelating ligands, reaction time, and acetone treatment are also critical to obtain the apatite structures. Especially, multifunctional strontium hydroxyapatite nanorods with luminescent and mesoporous properties can be easily synthesized at a low temperature, and have good biocompatibility, stability, nontoxicity, and water-soluble properties.¹⁰⁶

In addition, the defect-related fluoride materials prepared by the solvothermal method were also reported.^{97,110} The as-obtained alkaline earth metal fluoride (CaF_2 , SrF_2 , BaF_2) nanocrystals based on the solvothermal method exhibit a narrow size distribution, and can be well dispersed in nonpolar solvents. The colloidal solutions of these three fluoride nanocrystals dispersed in cyclohexane present a strong emission

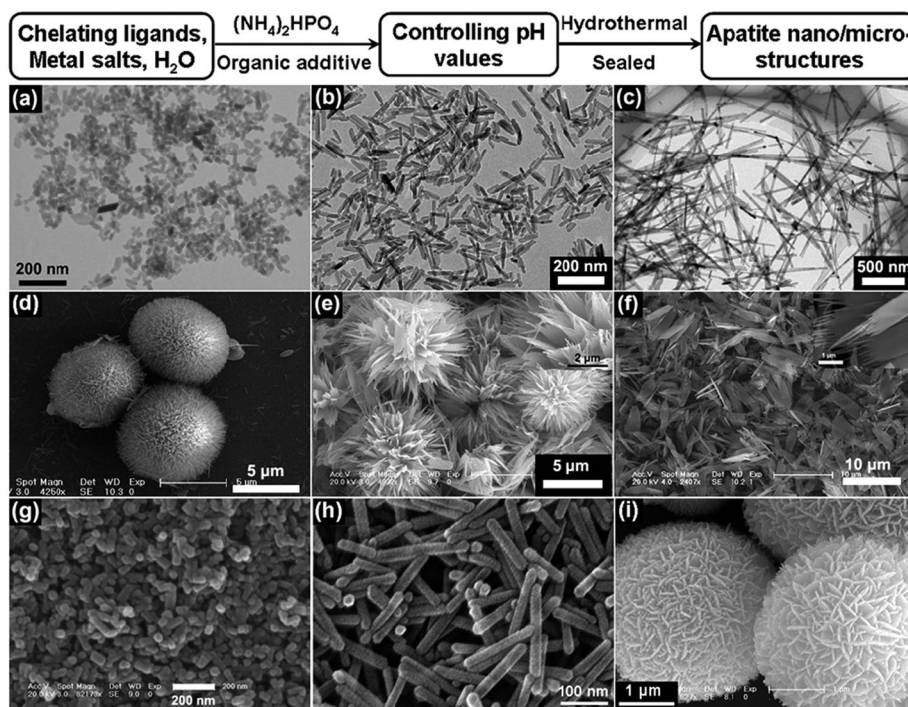


Fig. 2 The general synthetic methodology for a series of apatite nano/microstructures by hydrothermal method and the typical methodologies for defect-related luminescent apatite structures by hydrothermal method. Typical TEM and SEM images of calcium hydroxyapatite (a–f) (reproduced with permission from ref. 103, copyright 2009, American Chemical Society), SEM images of calcium fluorapatite (g) (reproduced with permission from ref. 105, copyright 2010, Royal Society of Chemistry), and strontium hydroxyapatite (h, i) (reproduced with permission from ref. 106 and 104, copyright 2010, 2009, Elsevier and American Chemical Society) with multiform shapes.

band around 400 nm in the PL spectra.⁹⁷ In addition, a series of well-dispersed KRE₃F₁₀ (RE = rare earth: Sm–Lu, Y) colloidal nanocrystals with a rich variety of morphologies, such as hexagonal nanoplates, nanocubes and nanoparticles have been synthesized by a facile solvothermal route. The as-prepared nanocrystals are highly crystalline and can be well dispersed in nonpolar solvents such as cyclohexane and chloroform to form stable and clear colloids, which all display self-activated luminescence.¹¹⁰

2.3. Hydrolysis method

It is well known that the hydrolysis method is often used to prepare hydroxide and oxide materials using alkoxides as precursors. Over the past decade, monodisperse nano-/microspheres, which exhibit tunable or size-dependent photoluminescent properties, have been synthesized by the hydrolysis method and extensively investigated.^{111–115} Our group has reported the simple synthesis of nearly monodisperse zirconia spheres (ZrO₂) with defect-related tunable luminescent properties (Fig. 3a and b) by the controlled hydrolysis of zirconium butoxide in ethanol, followed by heat treatment in air at low temperature from 300 to 500 °C.^{106,116}

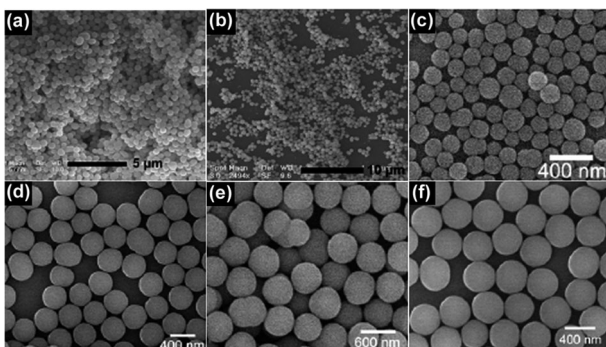


Fig. 3 Typical SEM images for unannealed ZrO₂ (a), heat-treated ZrO₂ spheres (b) (reproduced with permission from ref. 112, copyright 2009, American Chemical Society), and (c–f) SiO₂ spheres with different size (reproduced with permission from ref. 114, copyright 2010, Elsevier).

In addition, the well-known Stöber method,¹¹⁷ based on hydrolysis of tetraethylorthosilicate (TEOS) in an alcohol medium in the presence of water and ammonia, has been extensively employed to prepare the monodisperse silica (SiO₂) spheres with different sizes by a modified procedure (Fig. 3). These monodisperse SiO₂ spheres could be further annealed at low temperature (generally less than 600 °C), and exhibited bright, stable, and tunable defect-related luminescence.^{111,113} Apart from the methodology presented by Stöber and modified Stöber methods, other hydrolysis-related strategies have recently been developed, based mainly on reverse microemulsions using a stable and macroscopically isotropic dispersion of a surfactant and water in a hydrocarbon (Fig. 3c),^{114,118,119} or on direct micelles as templates.^{120,121}

2.4. Electrospinning process

The electrospinning technique was developed for the synthesis of one-dimensional (1D) nanomaterials.^{122–128} During the synthesis process, the as-synthesized 1D precursor needs to be annealed to remove the organic additives. Moreover, it is also possible to form some carbon-related impurities induced by residual organic additives and other oxygen-related defects as emission centers during the annealing process. Recently, the electrospinning method was employed to prepare multifunctional silica fibers, which possess irregular porous structure, and display fiber-like morphology with dimensions of several hundred nanometers in width and several millimeters in length (Fig. 4).¹²⁹ Furthermore, the as-obtained silica fibers exhibit an intense broad bluish emission, which might be attributed to impurities and/or defects in the silica fibers.

In addition, Qiu and co-workers reported tunable emission of BCNO nanoparticle-embedded polymer electrospun nanofibers.¹³⁰ Firstly, BCNO nanoparticles were prepared by a low-temperature method. Then, the BCNO nanoparticle-embedded polymer electrospun nanofibers were synthesized by an electrospinning process using synthesized BCNO phosphors as raw materials. Photoluminescence properties of these nanofibers indicate that the emission can be readily tuned by adjusting the C concentration in the BCNO phosphors.

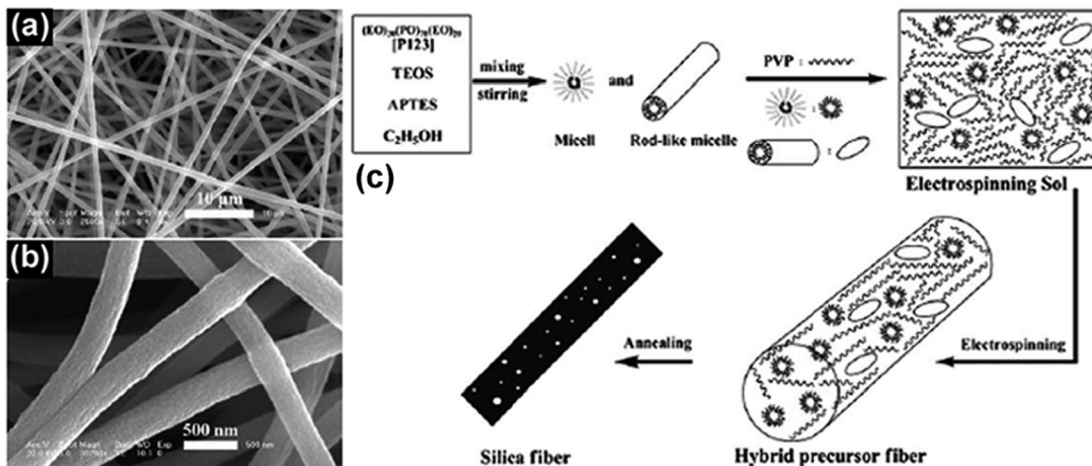


Fig. 4 Typical SEM images of the as-formed precursor (a) and porous silica fibers annealed at 600 °C (b). The possible formation process of the porous structures in silica fibers (c) (reproduced with permission from ref. 129, copyright 2010, Wiley).

2.5. Sonochemical synthesis

The sonochemical method has been widely used to prepare a variety of nanostructured materials.^{131,132} During the sonication process, propagation of pressure waves is intense enough to cause the formation, growth and implosive collapse of bubbles in liquid medium. These bubbles generate localized hotspots, which exhibit extreme temperatures, pressure and high cooling rates.¹³³ Sonochemical effects can primarily drive a variety of chemical reactions such as oxidation, reduction, and so on. During this special process, some defects can also be formed as a result of localized hotspots. Recently, Uchino and co-workers¹³⁴ synthesized luminescent silica crystals without luminescent activator ions *via* a sonochemical reduction route. The neutral oxygen vacancy or the F center induced by the sonochemical process might be the emission centers and give a broad visible PL band peaking at ~ 500 nm under UV irradiation. The sonochemical reduction of TEOS by a colloidal solution of sodium performed by Gedanken's group led to the formation of silicon.¹³⁵ Ultrasound-induced reduction was further applied to a system with silicon alkoxides and colloidal sodium to prepare luminescent silicon nanoparticles.

2.6. Chemical vapor deposition

The chemical vapor deposition (CVD) system is believed as an important synthesis method with several advantages, such as relatively low temperature and low cost, adaptable to a wide variety of structures, rapid growth, and direct growth on a large number of substrates.¹³⁶ Controlling the different reaction conditions (such as substrate temperature, pressure, reactant composition, reactant pre-treatment, supply rates, *etc.*), a number of forms of CVD are in wide use, including atmospheric pressure CVD (APCVD), aerosol-assisted CVD (AACVD), plasma-enhanced CVD (PECVD), and so on.^{137–139} So far, a large number of compounds, including oxides, sulfides, semiconductors, carbon-based materials, *etc.*, have been grown by these CVD methods.¹⁴⁰ Among them, some defect-related luminescent materials can also be obtained by this kind of method. Previously, off-stoichiometric silicon oxide (SiO_x , $x < 2$) thin films can often be synthesized *via* chemical vapor deposition.^{141,142} In addition, Becher's group reported the fluorescence and polarization spectroscopy of single silicon vacancy centers in heteroepitaxial nanodiamonds on iridium using microwave plasma chemical vapor deposition.¹⁴³ Yang and co-workers have successfully fabricated the In_2O_3 – ZnO one-dimensional nanosized heterostructures constructed by In_2O_3 quadrangular columns and ZnO hexagonal disks by thermal chemical vapor transport.¹⁴⁴

Besides the above methods, multistep heat treatment,¹⁴⁵ thermal decomposition,¹⁶ flame spray pyrolysis,¹⁴⁶ microwave irradiation method,¹⁴⁷ *etc.* can also be employed to prepare the defect-related luminescent materials.

3. Classification and optical properties

Defect-related luminescent materials can be classified into silica-based materials, phosphate systems, metal oxides, BCNO phosphors, and carbon-based materials, *etc.* Here we will elucidate the luminescent properties together with their

control and tuning, and emission mechanisms (solid state physics) of these materials.

3.1. Silica and silica-based materials

Earlier defect-related luminescent materials were mainly based upon silica and silica-based materials, including silicate-carboxylate,¹⁷ SiO_2 glass,^{18,22} SiO_2 gels,^{27,28} SiO_2 spheres,^{111,114} organic/inorganic hybrid silicones,^{23–25} silica nanotubes,¹⁴⁸ molecular sieves,^{31,149} *etc.*^{150–156} As the most promising materials for environmentally friendly phosphors, these kinds of luminescent materials have been the focus of research efforts since the pioneering work of Sailor and co-workers.^{17,121} It has been reported that a kind of white phosphor with high emissive broadband spectra (Fig. 5a) (emission maximum between 450 and 600 nm) can be synthesized from a sol–gel precursor and a variety of organic carboxylic acid with a low heat treatment. The PL quantum yield of these materials ranged from 20% to 45% under UV (365 nm) excitation with PL lifetime less than 10 ns. In addition, it is worth pointing out that the bright white photoluminescence was first attributed to carbon defect centers and the detailed scheme of the carbon substitutional defect for Si as the luminescent species in the lattice is shown in Fig. 5b. Apart from this, silica gels have been also extensively investigated as defect-related phosphors. Among them, silica aerogels, which are well-known to show photoluminescence generally from the blue to red spectral regions, exhibited several structural defects advantageous to photoluminescent properties, such as a non-bridged oxygen hole center (NBOHC) (described as $\text{SiOH} \rightarrow \text{SiO}^\bullet + \cdot\text{H}$; this defect was connected with bands at 1.8 and 1.9 eV),^{151–153} peroxy linkage (POL) (labeled as ROO^\bullet , where R represents an unspecified radical or part of the structure),¹⁵⁴ and E' center ($\equiv\text{Si}^\bullet$) on the basis of the basic emission characteristic band at 2.2 eV in the PL spectra.^{152,156} In addition, Hinić's group has reported PL spectra measured

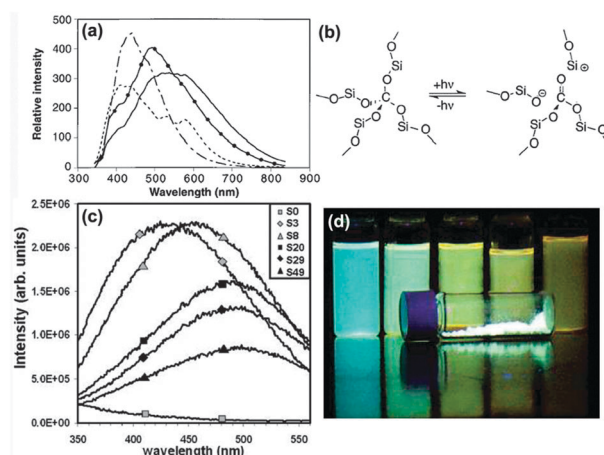


Fig. 5 Optical characterization of SiO_2 -based materials. Emission spectra (337 nm excitation at 298 K) of sol–gel-prepared SiO_2 -based phosphors (a) and a scheme of the carbon substitutional defect for Si as the luminescent species in the lattice (b) (reproduced with permission from ref. 17, copyright 1997, sciencemag.org). Emission spectra of monodisperse SiO_2 spheres excited at 300 nm (c) and the corresponding photographs (d) under a 365 nm lamp (reproduced with permission from ref. 111, copyright 2006, American Chemical Society).

for two series of silica aerogel sintered at 1000 °C for different time intervals. The photoluminescence band at 1.8 eV for silica aerogels originates from non-bridged oxygen hole center defects, and that at 2.0 eV originates from silane in the gel network.⁸²

The earlier research of silica/silica-based luminescent materials was mainly focused on the luminescent, physical, and chemistry properties. However, the luminescent properties can also be tailored by the size, shape, and composition. For example, the spherical morphology with narrow size distribution for phosphors is good for high brightness and high resolution because high packing densities and low scattering of light can be obtained by using such phosphors.^{79,157–161} Therefore, morphology-controlled silica-based luminescent materials have appeared over the past decades. The controlled preparation of colloidal silica was proposed for the first time by Kolbe in 1956 and then developed by Stöber *et al.* in the late 1960s.¹¹⁷ Based on modified Stöber procedures and following a heat treatment, Schmedake's group has reported a novel approach to synthesize mono-disperse luminescent silica spheres.¹¹¹ The tunable luminescent properties of the silica spheres depend on the quantity of (aminopropyl)triethoxysilane in the precalcined material (Fig. 5c). The possible luminescent mechanism was ascribed to carbon/oxygen-related defect centers resulting from calcination of the APTES-containing SiO₂ spheres. Luminescent and porous silica fibers prepared by the electrospinning process have also been extensively investigated.¹²⁹ These kinds of multifunctional silica fibers showed a strong self-activated photoluminescence ranging from 300 to 600 nm (centered at 405 nm), which might be caused by impurities and/or defects in the silica lattice. Moreover, molecular sieves with porous structure (such as MCM-41³¹ and MCM-48³²) also show excellent and tunable luminescent properties in the visible region. Most recently, as particularly interesting nanomaterials, luminescent silica nanoparticles were developed by Davies *et al.* based on the aqueous sol–gel technique.⁷⁸ The as-obtained silica nanomaterials without metal activators or traditional dyes displayed a broad white emission. They also proposed that the source of emission was from the formation of hydrocarbon-based defects during synthesis, which originated from the alkoxysilane used to prepare the nanostructures.

Due to the good optical properties, high chemical stability, and nontoxicity, the applications of these multifunctional SiO₂-based materials have extended in biomedicine fields. Therefore, innovative research is ongoing in the silica-based defect-related phosphors. Clearly, we cannot exhaustively cover this field, so our efforts here are to highlight the recent studies. In the above silica-based materials, a summary description of general properties and luminescent mechanisms for silica-based materials is listed in Table 1.

3.2. Phosphate system

3.2.1. BPO₄-related system. The crystal structure of BPO₄ is built by sharing the corner of the BO₄ and PO₄ tetrahedra, leading to a continuous three-dimensional framework, which is isomorphous with silica oxides. This information told us that BPO₄-based materials might be another kind of defect-related phosphor. Our group firstly reported the luminescent properties of BPO₄-based materials prepared by PSG method.^{86–88} This

PSG-derived BPO₄ can show a weak purple emission under UV irradiation, which may be caused by the carbon impurities in the host lattice (Fig. 6a and e). In further study, when a slight amount of alkali metal or alkaline earth metal ions (Sr²⁺, Ca²⁺, Mg²⁺, Ba²⁺ Li⁺, Na⁺, or K⁺) were doped into the BPO₄ host lattice, the luminescent intensities can be enhanced (Fig. 6a, b and 7A), which are due to the oxygen-related defects (peroxy radical defects or oxygen vacancy) (Fig. 6d).^{86,87} As structural disturbance of BPO₄ by dopants can create more defect centers in BPO₄-based systems, especially BPO₄/Ba²⁺ and BPO₄/Li⁺, leading to be the most efficient phosphors (Fig. 6e and 7A). The energy band diagram of the possible defects and emission process in sol–gel-derived BPO₄ and BPO₄/Ba²⁺ was also investigated (Fig. 6f and 7D). The possible luminescent mechanisms (carbon impurities, peroxy radical defects, or oxygen vacancy) for these kind of phosphors were first proposed in BPO₄-based materials. In addition, the BPO₄–xSiO₂ (x: SiO₂/BPO₄ molar ratio, 0–70%) and BPO₄–xAl₂O₃ (x: Al₂O₃/BPO₄ molar ratio, 0–20%) hybrid systems prepared by the PSG process are also stable, efficient, and defect-related luminescent materials.⁸⁸ Furthermore, the doping/mixing concentration, annealing temperature, and the amount of additives in the precursors also have a great effect on the defect-related luminescent properties of BPO₄-based materials (Fig. 7B and C). And the band structures of defective BPO₄, which were employed to further investigate the defect-related luminescent mechanisms, were calculated using CASTEP code based on density-function theory (DFT). In this calculation, the structure models of ideal and defective [interstitial carbon (C_i) and oxygen vacancy (V_O)] BPO₄ are established (Fig. 7D). The band gaps for ideal and defective BPO₄ are calculated based on the corresponding models (Fig. 7D). The calculated results indicated that both the C_i and V_O can cause great change in the band structure (size of band gap, site of conduction band and valence band, and band structure), which can well explain the luminescence phenomenon and the proposed mechanisms. Therefore, the analysis of the band structure can offer a valuable alternative to investigate the luminescent mechanisms of defect-related luminescent materials.

3.2.2. Apatite-structured materials. It is well known that apatite-structured materials, including HAp, SrHAp, FAP, etc., are regarded as a typical class of biological materials due to their super-biological stability, biocompatibility, and affinity. Obviously, these kinds of nano/micromaterials with excellent fluorescence may serve as ideal candidates for biomedicine applications, such as cancer diagnosis, drug delivery, and so on. Therefore, they have attracted widespread attention. In earlier research, the luminescence of apatite structure materials is usually realized by depositing optically active rare-earth-doped nanophosphors (*i.e.*, Y₂O₃:Eu³⁺ nanoparticles) on the surface or doping the materials with lanthanide/transition metal ions.^{56,127,162,163} However, the lanthanide/transition metal ions are often expensive and non-environmentally friendly elements, which may have toxic effects.

In the past few years, much effort has been put into the investigation of defect-related luminescent properties in apatite materials. Defect-related apatite materials have been successfully

Table 1 Summary comparison of the defect-related silica-based luminescent materials

Materials	Fabrication route	Excitation	Emission	Possible mechanism	Ref.
Silicate-carboxylate SiO ₂ glass	Sol-gel method	365 nm	Broad and maximum between 450 and 600 nm	Carbon substitutional defect	17
	Sol-gel method	UV excitation at 337.1 nm	Broad emission, maxima at 420 and 520 nm (500 °C)	Defects of oxygen deficiencies (420 nm), radical carbonyl defects (520 nm)	18
		Peaking at 360 and 225 nm	Entire visible spectrum, peaking at 425 and 500 nm	Chemical bond cleavage and resultant carbon formation and/or non-stoichiometry	22
SiO ₂ gels	Vapor phase axial deposition	Absorption at 3.8 eV (oxygen plasma process)	1.9 eV luminescence	NBOHC (1.9 eV PL) and peroxy linkage (3.8 eV)	154
	Sol-gel method	355 nm	Blue luminescence	O ₂ ⁻ species	27
SiO ₂ spheres	Similar to Stöber method	Broad band peaking at 363, 236, 243 nm	Broad band (360-600 nm)	Carbon impurity mechanism	28
		300 nm	Maximum red-shifted with increasing APTES concentration	Carbon/oxygen-related defect center	111
Organic/inorganic hybrid silicones	A water/oil microemulsion method and Stöber method	Broad band ranging from 280 to 400 nm	Broad emission and maximum between 385 and 470 nm,	Carbon impurities and oxygen defects	114
		330, 350, 365, 395, 365, 400, and 420 nm	Emission spectra are excitation wavelength dependent	Emission originated in the NH (NH ₂) groups of the urea or urethane bridges with electron–hole recombinations	23
	Sol-gel method	Broad band, depending on monitored emission wavelengths	Broad band between 350 and 680 nm	NH-related emission	24
SiO ₂ nanotubes	Reverse-microemulsion mediated sol-gel method	Broad band between 315 and 450 nm, recorded at 462 nm	Broad and red shift with the decrease of excitation energy	Recombination electron–hole mechanisms	25
		350 nm	Three emission bands at 410, 435 (maximum), 460 nm	Intrinsic diamagnetic centers (O-Si-O, violet emission) and neutral oxygen vacancy (\equiv Si-Si \equiv , blue emission)	148
		350, 300, 250, and 200 nm	420, 473, and 620 nm	Oxygen-related defect sites	31
Molecular sieves	Siliceous synthesis gel	365 nm	Blue emission	Oxygen-related defects (\equiv Si-O \bullet) in MCM-41 series	149
	Hydrothermal process and following heat treatment	350, 300, 250, and 200 nm			
SiO ₂ nanowires	Heating method	Two excitation bands at 260 (4.77 eV) and 368 nm (3.37 eV)	Broad PL band at 443 nm (2.8 eV) with a shoulder at 413 nm (3.0 eV)	Defects	150
Silica fibers	Electrospinning process	A double broad band (200–370 nm) peaking at 255 and 355 nm	PL emission ranging from 300 to 600 nm and maximum at 405 nm	Impurities and/or defects in the silica lattice	129
Silica nanoparticles γ-Irradiated α-SiO ₂	Sol-gel technique	457 nm	Broad white emission	Hydrocarbon-based defects	78
	Plasma CVD method	Excited by 2–4 eV photons	Two bands at 1.9 eV and 2.2 eV	Nonbridging oxygen hole centers (1.9 eV PL) and E' centers (2.2 eV PL)	152
Silica aerogels	Two-step acid-base catalyzed process	300–400 nm	Emission wavelength ranges from 460–500 nm	Oxygen defect centers in the aerogel matrix	155
	Calcination	Excited by a 488 nm (2.54 eV) Ar ion laser	Three PL bands at 1.8, 2.0 and 2.2 eV	Nonbridged oxygen hole center defect (1.8 eV) and silane in gel network (2.0)	82
Silicon-rich oxynitride (SiO _x N _y :H)	Plasma-enhanced chemical vapor deposition	Excited in the range of 2.4–3.8 eV	A broad tunable PL emission	Silicon suboxide bonding (E' centers)	156

synthesized by a facile hydrothermal process. The as-obtained samples showed strong blue emission with controllable morphologies and structures (Fig. 8).^{103–106} Here we take the preparation and properties of HAp and SrHAp phosphors as representative examples to illustrate the advantages of the defect-related apatite materials. The hydrothermal-derived HAp samples with trisodium citrate in the precursor can show an intense and bright blue emission under long-wavelength UV light excitation (341 nm). This emission spectrum consists of a strong broad band ranging from 350 to 570 nm with a maximum at 414–434 nm (Fig. 8a).¹⁰³ The corresponding excitation

spectrum of the HAp burr-like microspheres includes two broad bands: a weak band from 200 to 280 nm and a very strong and broadband from 280 to 420 nm (Fig. 8b), which can be excited by a wide range of UV light. It is presumed that CO₂ \bullet ⁻ radical impurities in the crystal lattice may play a key role for the luminescent properties, based on the results of the analysis and experiments such as Fourier transform infrared (FT-IR) spectra, EPR, and control experiments. These defect centers induce an electron localized in the 2p orbital of the single bonded carbon, which can give rise to photoluminescence through a strong electron-photon coupling.^{43,88}

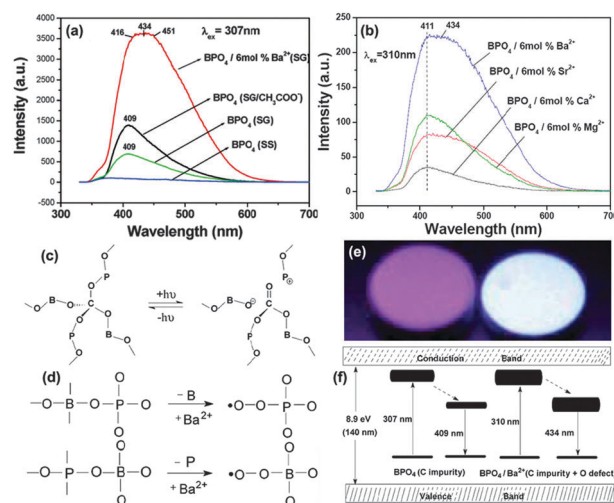


Fig. 6 (a, b) Emission spectra for BPO₄ and BPO₄ doped with alkaline earth metal ions [SG = sol-gel; SG/CH₃COO⁻ = sol-gel with CH₃COONH₄ instead of Ba(CH₃COO)₂ as dopant; SS = solid-state reaction using H₃BO₃ and (NH₄)₂HPO₄]. (c) Scheme of excitation and emission process induced by C impurities in BPO₄. (d) Scheme of the production of peroxy radicals in BPO₄ by Ba²⁺. (e) Photographs of the sol-gel-derived BPO₄ and BPO₄/6 mol% Ba²⁺ phosphor pellets under a UV (365 nm) lamp in the dark. (f) Energy band diagram showing the possible defects and emission process in BPO₄ and BPO₄/6 mol% Ba²⁺ (reproduced with permission from ref. 86, copyright 2006, American Chemical Society).

Upon further investigation of the luminescent properties, it can be found that HAp samples with different morphologies

show different emission intensities (Fig. 8a). Among them, HAp microspheres show the strongest blue emission and HAp nanocrystals exhibit the weakest luminescence. The as-obtained HAp microspheres have higher crystallinity, and spherical morphology is good for high brightness and high resolution because of high packing densities and low scattering of light.⁷⁹ Based on the above situation and consideration, other important apatite structures of FAP nanomaterials¹⁰⁵ and SrHAp samples with different size and morphologies were also obtained. The luminescent properties of the SrHAp can be tuned by the reaction time and the molar ratio of metal ions and chelating ligands. Normally, the photoluminescence intensity first increased with increasing the reaction time, reached a maximum at a certain time, and then nearly kept the maximum with further increase of reaction time (Fig. 8c). This might be due to the improvement of the crystallinity.¹⁰⁴ On the other hand, the photoluminescence intensity varied with the change of the molar ratio of metal ions and trisodium citrate (Fig. 8d). At a high molar ratio, the emission intensity decreased greatly, which may be caused by the quenching effect of the luminescent centers. This luminescence study can confirm the key role of trisodium citrate on the luminescence properties.¹⁰⁶ The comparison of luminescent properties and mechanisms of these defect-related phosphate phosphors are summarized in Table 2.

3.3. Metal oxides

Metal oxides now represent the most mature luminescent materials, which can be classified into two major categories: metal activator-doped metal oxide phosphors (*e.g.* Y₂O₃:Eu³⁺)

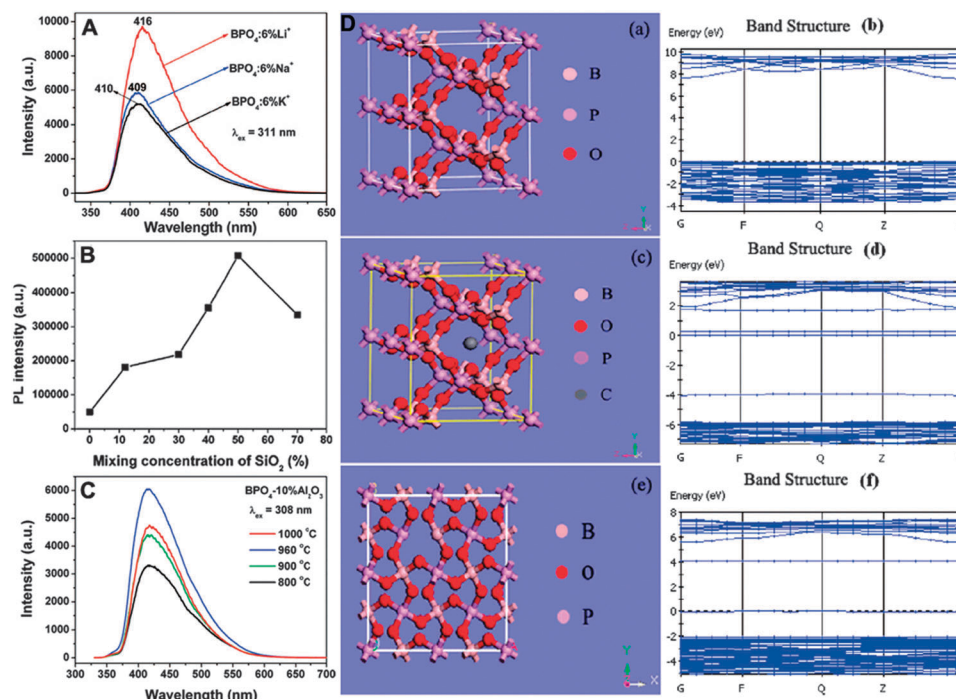


Fig. 7 (A, B, C) Luminescent properties of the BPO₄-based materials affected by dopants, concentration, and temperature. (D) Structure models of BPO₄: ideal (a), interstitial carbon (c), oxygen vacancy (e), and the calculated band structures according to models of ideal BPO₄ (b), interstitial carbon-defective BPO₄ (d), and oxygen vacancy defective BPO₄ (f) (reproduced with permission from ref. 87 and 88, copyright 2009, 2008, American Chemical Society).

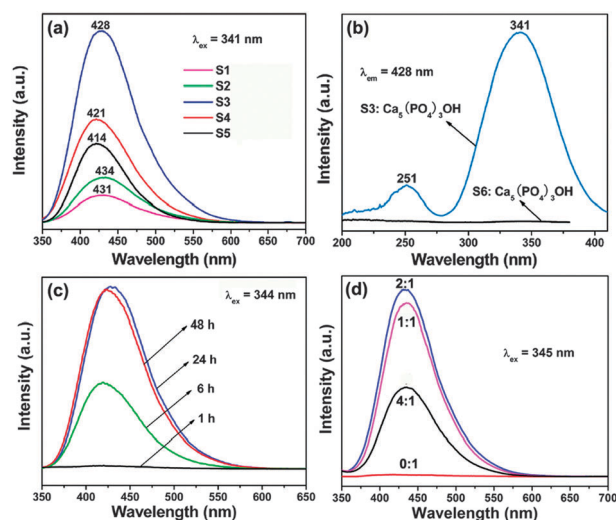


Fig. 8 (a) PL emission spectra of hydrothermal-derived HAp samples (S1: nanorods and nanoparticles obtained at pH = 9.0, S2: nanorods obtained at pH = 7.0, S3: burr-like microspheres obtained at pH = 5.0, S4: microflowers obtained at pH = 4.5, and S5: microsheets obtained at pH = 4.0). (b) PL excitation for HAp sample S3 (reproduced with permission from ref. 103, copyright 2009, American Chemical Society). (c) Emission spectra of SrHAp samples obtained from different reaction times (reproduced with permission from ref. 104, copyright 2009, American Chemical Society). (d) Emission spectra for the SrHAp samples prepared with different molar ratios of $\text{Cit}^{3+}/\text{Sr}^{2+}$ (reproduced with permission from ref. 106, copyright 2010, Elsevier).

and defect-related materials. For the defect-related metal oxide phosphors, the species, synthesis, properties, and luminescent mechanisms are classified and listed in Table 3.

Table 2 Summary comparison of the defect-related phosphate-system luminescent materials

Materials	Fabrication route	Excitation	Emission	Possible mechanism	Ref.
$\text{BPO}_4/\text{Ba}^{2+}$ (Sr^{2+} , Ca^{2+} , and Mg^{2+})	PSG process	Broad band (220–450 nm) with maximum at 310 nm	Bluish-white emission band peaking from 416 to 451 nm	Carbon impurities and oxygen-related defects	86
Alkali metal ion-doped BPO_4	PSG process	Broad band (220–400 nm) peaking at 311 and 375 nm	Strong emission (360–570 nm, $\text{BPO}_4:6\%\text{Li}^+$ maximum at 416 nm)	Carbon impurities and oxygen vacancy (V_O^\bullet center)	87
$\text{BPO}_4-\text{SiO}_2-\text{Al}_2\text{O}_3$ mixture	PSG process $\text{BPO}_4-x\text{SiO}_2$	One broad band with a maximum at 313 nm	Emission band centered at 428 nm, SiO_2 concentration and annealing temperature dependent	Carbon impurities and oxygen vacancy (V_O^\bullet center)	88
	PSG process $\text{BPO}_4-x\text{Al}_2\text{O}_3$	Two broad bands peaking at 308 and 372 nm	Emission band centered at 413 nm, Al_2O_3 concentration and annealing temperature dependent	Carbon impurities and oxygen vacancy (V_O^\bullet center)	88
Hydroxyapatite $\text{Ca}_5(\text{PO}_4)_3\text{OH}$ nano/microcrystals	Hydrothermal process	A weak band (200–280 nm) and a strong broadband (280–420 nm)	Blue emission (350–570 nm) and morphologies dependent	Carbon dioxide radical ($\text{CO}_2^\bullet-$)	103
Strontium hydroxyapatite	Hydrothermal process (microsphere) Hydrothermal process (nanorods)	Long-wavelength UV light excitation (344 nm). Two broad bands peaking at 254 and 345 nm	Blue emission centered at 427 nm Blue emission and dependent on cumulatively released amount of drug	Carbon dioxide radical ($\text{CO}_2^\bullet-$) Carbon dioxide radical ($\text{CO}_2^\bullet-$)	104 106
Mesoporous silica/apatite composite	Modified Pechini sol-gel process	Two bands centered at 280 and 330 nm	Blue luminescence (maximum at 410 nm)	Carbon dioxide radical ($\text{CO}_2^\bullet-$)	90
Calcium fluorapatite	Hydrothermal process	Broad excitation band (200–400 nm)	Blue emission $\text{Ca}_5(\text{PO}_4)_3\text{F}$	Carbon dioxide radical ($\text{CO}_2^\bullet-$)	105
			White emission color for Ce^{3+} , Mn^{2+} -codoped $\text{Ca}_5(\text{PO}_4)_3\text{F}$ excited by 308 nm UV light	Carbon dioxide radical ($\text{CO}_2^\bullet-$) and Ce^{3+} , Mn^{2+} activators emission	

3.3.1. Zirconia. Zirconia (ZrO_2) is an important ceramic material and widely used in high-performance ceramics, catalysts, cosmetics, and new emergent applications of high-temperature fuel cells and bioceramics (such as dental prostheses). Along with the further investigation on phosphors, some attention has been paid to the luminescence properties of ZrO_2 .¹⁶⁴ During the early study, Li and co-workers reported that tetragonal ZrO_2 nanoparticles synthesized by a microwave irradiation method showed sharp emission peaks at 402, 420, and 459 nm under 254 nm UV excitation and a broad-band emission at 608 nm under 412 nm UV excitation.¹⁴⁷ The ZrO_2 nanocrystals prepared by a two-phase process presented by Zhao *et al.*¹⁶⁵ exhibited a broad-band emission with a maximum at 365 nm under UV excitation (250 nm). These reports indicated that the luminescence intensity of ZrO_2 nanocrystals seemed to depend strongly on the preparation method. Moreover, the luminescent mechanisms need to be further investigated and clarified.

In a further study, Lin and co-workers⁴³ have found that PSG-derived nanocrystalline ZrO_2 powders annealed at 500 °C and crystallized as tetragonal could exhibit white-blue emission centered at 425 nm under a wide range of UV light excitation, which is suitably excited by different light sources. By further increasing the annealing temperature, the phase transformation of ZrO_2 from tetragonal to monoclinic occurs. The monoclinic ZrO_2 samples could give an intense blue-green emission (470 nm) after being annealed at 1000 °C (Fig. 9A). This result confirmed that the phase of the phosphor can affect the emission color and/or luminescent intensity. Moreover, the detailed study indicated that the whitish blue and blue-green emission bands can be ascribed to interstitial carbon defects (C_i) in the tetragonal ZrO_2 and oxygen defects in the monoclinic ZrO_2 , respectively.⁴³ The PSG-derived ZrO_2 presented

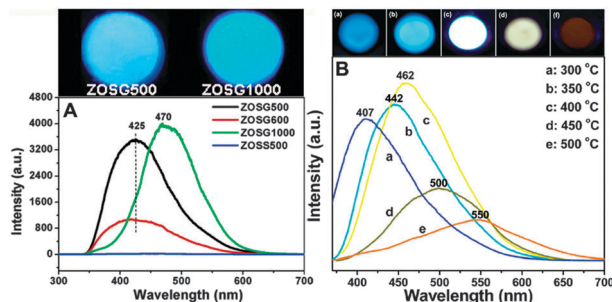


Fig. 9 (A) Photographs under UV light from mercury lamp in a dark room and corresponding emission spectra of the ZrO₂ crystals annealed at different temperature (ZOSG: ZrO₂ *via* sol–gel process; ZOSS: ZrO₂ *via* the solid-state reaction). (B) Luminescence photographs under a 365 nm UV lamp and emission spectra of ZrO₂ annealed at different temperature (reproduced with permission from ref. 38 and 112, copyright 2007 and 2009, American Chemical Society).

strong and bright emission, however the high annealing temperature caused serious aggregation. Therefore, to avoid this situation, other methods to control the synthesis of ZrO₂ luminescent materials were explored. Well-dispersed ZrO₂ spheres with a narrow size distribution were successfully prepared by the controlled hydrolysis of zirconium butoxide in ethanol. With a subsequent heat treatment in air at low temperature (300–500 °C), the annealed ZrO₂ spheres exhibited broad, intense, and visible photoluminescence (Fig. 9B).¹¹² Moreover, the emission colors of the ZrO₂ spheres can be tuned from blue to nearly white to dark orange by varying the annealing temperature. Based on the spectral analysis, luminescence lifetimes, and EPR results, the luminescent centers might be attributed to the carbon impurities in the ZrO₂ lattice. And the concentration of the carbon impurities is closely related with the annealing temperature and the amount of the organic additive.

Based on these researches, defect-related luminescent properties of ZrO₂ and ZrO₂-based phosphors can be influenced by synthesis method, species of defect, phase, and surface/interface properties. By controlling these factors, many defect-related ZrO₂ phosphors with different emission color or intensity could be achieved, which enriches the inorganic luminescent materials and provides novel phosphors as alternatives to traditional phosphors.

3.3.2. Alumina. Cai *et al.* and Chen *et al.* found photoluminescence properties in porous alumina membranes.^{166,167} Zhang *et al.* reported a blue luminescence from amorphous Al₂O₃ nanoparticles suspended in toluene solution through ultrasonic treatment of a porous anodic alumina membrane.¹⁶⁸ From an earlier study, it was found that the intense blue emission of as-obtained nanoparticles strongly depended on the particle size and chosen solvent. Moreover, a mixed mechanism combining the surface bonding states with widened bandgaps of alumina nanoparticles by the quantum confinement effect is presented.¹⁶⁸ In a follow-up study, our group also demonstrated the amorphous Al₂O₃ powder samples prepared by the PSG process and annealed at 500 and 600 °C exhibited bright bluish-white emission centered at 430 and 407 nm, respectively.⁸⁹ The most probable luminescent center was ascribed to radical carbonyl defects such as $\equiv\text{Al}-\text{O}-\text{C}^{\bullet}=\text{O}$ on the pore surface.

Besides the defect-related Al₂O₃ phosphors, the Al₂O₃–SiO₂ porous glasses with high luminescence quantum efficiencies have also been well investigated by Hayakawa *et al.* Further investigation of Al₂O₃–SiO₂ porous glasses indicated that the Al₂O₃ content could affect the luminescent properties.¹⁸ More recently, Raubach and co-workers reported interfacial photoluminescence emission properties of core/shell Al₂O₃/ZrO₂. In their research work, the general aspect of the spectra is a broad band ranging from 350 to 620 nm (maximum at 455 nm), which covered a large part of the visible light. A possible mechanism was ascribed to the multi-photonic process based on the recombination of excited electrons and holes. Interestingly, PL spectra ($\lambda_{\text{ex}}=350.7$ nm) also revealed that the effect of the zirconia coating on the alumina was more effective for α -Al₂O₃ than for γ -Al₂O₃, which may be related to the process of coating zirconia on alumina.¹⁶⁹

3.3.3. Rare earth oxides. Rare earth oxides have been extensively used in high-performance luminescent devices, magnets, catalysts, and other functional materials because of their electronic, optical, and chemical characteristics resulting from the 4f electronic shells. However, most rare earth oxide phosphors are metal activator-doped materials, for example traditional red phosphor Y₂O₃:Eu³⁺. Research on defect-related rare earth oxide phosphors could decrease the amount of rare earth ions, particularly very expensive rare earth activators (such as Eu³⁺, Tb³⁺, Er³⁺, Dy³⁺, etc.), which would greatly reduce the cost and increase safety for the environment and people's health. As a result, defect-related luminescent materials without metal activators have attracted much attention.

Lin and co-workers have successfully synthesized Y₂O₃ powders *via* the sol–gel process using glycerol and polyethyleneglycol as additives, followed by low-temperature treatment.¹⁷⁰ The as-prepared Y₂O₃ sample shows intense bluish-white emission (350–600 nm) with a quantum yield as high as 64.6% under a wide range of UV light excitation (235–400 nm). These luminescent properties were caused by carbon impurities in the Y₂O₃ host. In addition, highly uniform and well-dispersed CeO₂ nanocrystals (3.5 nm in diameter) were prepared by a nonhydrolytic solution route.¹⁷¹ This kind of undoped CeO₂ can show a weak emission band with a maximum at 501 nm. The emission band is not due to the characteristic emission of the lanthanide ions but might arise from the oxygen vacancy which is introduced in the fluorite lattice of the CeO₂ nanocrystals to compensate the effective negative charge associated with the trivalent ions. In a further study, Tanner and Wang¹⁷² presented the intense and white upconversion luminescence from several rare earth oxides (Ln₂O₃, Ln = Sm, Tm, Yb, and CeO₂) excited by a 808 nm laser diode, which is unlike the upconversion spectra of lanthanide-ion activators. The color purity is excellent for the prepared oxides. Among them, the coordinates for neat Tm₂O₃ and Yb₂O₃ are close to those for pure white light. Moreover, they speculated that the mechanism involved thermally induced production of free carriers.

3.3.4. ZnO, SnO₂, and In₂O₃. As a wide-band-gap semiconductor, zinc oxide (ZnO) has been known as a luminescent material for a long time, and it is of great interest for photonic applications such as UV luminescent devices, low threshold

Table 3 Summary of the defect-related oxide luminescent materials

Representative examples		Synthetic method	Excitation	Emission	Possible mechanism	Ref.
ZrO_2	Nanoparticles	Microwave irradiation method	254 and 412 nm	Sharp emission excited by 254 nm and broad-band emission excited by 412 nm	Surface defects and oxygen vacancies	147
	Colloidal nanocrystals	Two-phase process	250 nm	Broad-band with a maximum at 365 nm	A mid-gap trap state induced by surface passivation.	165
	Nanocrystals	PSG process	302 nm	White-blue emission (tetragonal phase)	Interstitial carbon defects	43
			280 nm	Blue-green emission (monoclinic phase)	Oxygen defects	
$\text{Al}_2\text{O}_3-\text{ZrO}_2$	Spheres	Hydrolysis and followed by a heat treatment	365 nm	Tunable emission (blue-white-dark orange) by varying the annealing temperature	Carbon impurities	112
	Core-shell	Polymeric precursor method	350.7 nm	Broad band (350–620 nm)	Recombination of excited electrons and holes	169
Al_2O_3	Porous membrane	Electrochemical method	360 nm	Blue PL band (400–600 nm)	Singly ionized oxygen vacancies (F^+ centers)	166
	Two-step anodizing process		200–400 nm	Blue-emitting bands (420–600 nm) peaking at 452 nm	Oxygen defects and oxalic impurities	167
			330 nm	Broad band and a blue-shift as the decrease of particle sizes	Surface bonding energy levels and the oxygen defect levels	168
	Nanoparticles	Ultrasonic treatment	Broad band (235–425 nm)	Bluish-white emission (350–600 nm)	Carbon-related defect (radical carbonyl defect)	89
$\text{Al}_2\text{O}_3-\text{SiO}_2$	Porous glasses	Sol-gel method	337.1 nm	White light emission peaking at 420 and 520 nm	Oxygen defects and radical carbonyl-terminations	18
	Y_2O_3	PSG process	235–400 nm	Bluish-white emission (350–600 nm)	Carbon impurities	170
		Calcination	808 nm	Upconversion white luminescence	Thermally induced production of free carriers	171
CeO_2	Nanocrystals	Non-hydrolytic solution route	Broad band (280–420 nm)	Emission band with a maximum at 501 nm	Oxygen vacancy	172
ZnO		Polyol method followed by annealing, electrodeposition, chemical solution deposition, two-step process, molecular-beam epitaxy, or sol-gel process, etc.	UV light excitation for PL spectra or low-voltage electron beam excitation for cathodoluminescent spectra (CL)	Bright green luminescent	Interstitial oxygen ion (O_i^-), ionized oxygen vacancies (V_O^+), or Zn vacancy	176, 177, 182
				Violet luminescence	Defects associated with zinc or oxygen vacancies or vacancy related complexes	178, 179, 180
SnO_2	Nanorods	Hydrothermal method	295 nm	Yellow emission	Oxygen vacancy O_i^-	181, 182
	Nanowires	Vapor-liquid-solid process	Excitation power (0.5–10 mW)	Orange-red emission	Oxygen interstitials	183, 184, 185
	Nanoparticles	Sol-gel method	300 nm	Broad emission (350–550 nm)	Oxygen vacancies	187
	Hierarchical nanostructures	Multistep thermal vapor deposition	325 nm	Ultraviolet photoluminescence	Defect states	190
In_2O_3	$\text{In}_2\text{O}_3/\text{SiO}_2$	Soaking and thermal-decomposition	275 and 250 nm	Emission band centered at 400 nm	Oxygen vacancy ($\text{V}_\text{O}^{\bullet\bullet}$)	191
	Nanocubes	Hydrothermal treatment	380 nm	Blue-violet and yellow bands centered at 432 and 539 nm	Oxygen vacancies and structural defects	192
	Nanofibers	Solvothermal reaction	325 nm	Ultraviolet and visible emissions	Sulfur impurities and quantum size effect	194
	Nanorod bundles and spheres	Hydrothermal process	300–425 nm with a maximum at 383 nm	Blue-green emission centered at 450 nm	Oxygen vacancies	195
Nanocrystals		Solvothermal method	234 nm	Three emission peaks at 378, 398, and 420 nm	Oxygen vacancies	196
				Blue emission peaking at 416 and 439 nm	Oxygen vacancies	197
			Blue emission centered at 423 nm and size dependent	Weak quantum-confinement-effects	198	

lasers, nonlinear optical devices and so forth.^{173–175} ZnO is a famous defect-related phosphor which has good characteristics such as low outgassing, high electric conductivity ($\sim 10^{-3} \Omega \text{ cm}^{-1}$), low

excitation voltage, and high stability,¹⁷⁶ and has been extensively used as a bright green phosphor.¹⁷⁷ Besides the green emission, violet,^{178–180} yellow,^{181,182} and orange-red^{183–185}

emissions have been also observed and investigated. Since these emissions are located in a wide range of the visible spectrum, great efforts have been made to tailor these visible emissions.¹⁸⁶ As a representative example, ZnO and ZnO:Zn phosphors have been successfully synthesized by the polyol method followed by annealing in air and reducing gas, respectively, which showed tunable PL and cathodoluminescent (CL) properties.¹⁷⁶ In this research, the emission spectra of ZnO powders annealed at 950 °C in air contained a weak ultraviolet emission band at 390 nm and a broad emission band centered at about 527 nm, exhibiting yellow emission (Fig. 10a). However, when the sample was annealed in reducing conditions at temperatures from 500 to 1050 °C, the yellow emission decreased gradually and disappeared completely at 800 °C, whereas the ultraviolet emission band became the strongest. Above this temperature, the green emission (centered at 500 nm) appeared and increased with increasing reducing temperatures (Fig. 10b). Experimental results indicated that a singly ionized oxygen vacancy existed in the ZnO and ZnO:Zn powders (Fig. 10c). Based on the analysis, the yellow and green emissions may arise from the transitions of photogenerated electrons close to the conduction band to the deeply trapped hole in the single negatively charged interstitial oxygen ion (O_i^-) and the single ionized oxygen vacancy (V_O^\bullet) centers, respectively.¹⁷⁶ A schematic diagram of the radiative transitions responsible for emissions of these kinds of ZnO-based phosphors is shown in Fig. 10d.

Tin oxide (SnO_2) is another important metal oxide, which has an n-type wide band gap (3.6 eV at 300 K) but is dipole forbidden due to its special wave function symmetry.^{187–189} Furthermore, the exciton binding energy of SnO_2 is very large, which suggests efficient exciton emission at room temperature and even at higher temperatures. From the viewpoint of fundamental physics,¹⁹⁰ considerable research has been focused on the exploration of novel properties of SnO_2 nano-materials

(nanoparticles,¹⁹¹ nanowires,¹⁹⁰ nanorods,¹⁸⁷ hierarchical nanostructures,¹⁹² etc.), especially the photoluminescent properties. Photoluminescence of SnO_2 materials, generally observed in the UV and/or visible region (350–550 nm), may reveal the presence of crystalline defects (such as oxygen vacancies and tin interstitial or dangling bonds) resulting from various synthesis processes.^{187,190–192} Among them, oxygen vacancies have been assumed to be the most likely candidates for the recombination centers in emission processes for SnO_2 samples. Lü *et al.* presented the oxygen-vacancy-related photoluminescence of SnO_2 nanoparticles and the origin of the emission was assigned to the recombination of electrons in a conduction band with holes in the V_O^\bullet center.¹⁹¹ Another research group produced defect-related luminescent SnO_2 nanowires and proposed a different luminescent mechanism, which was identified: recombination of donor–acceptor pairs, excitons bound to neutral and ionized donor impurities, and optical transitions from free electrons to neutral acceptor impurities in the lattice.¹⁹⁰ In addition, Patra and co-workers have investigated the surface-defect-related luminescent properties of SnO_2 nanorods and nanoparticles.¹⁸⁷ This research work suggests that the luminescent properties can strongly depend on the shape. In conclusion, the emission of SnO_2 nanocrystals is due to a transition of an electron from a level close to the conduction band edge to a deeply trapped hole (V_O^\bullet) in the bulk of the SnO_2 nanocrystal and the surface-related defects are more prominent in smaller nanocrystals than in nanorods.

Similarly, indium oxide (In_2O_3) is also a very important wide-band-gap (direct band gap around 3.6 eV) and n-type transparent semiconductor due to its oxygen-efficient fluorite structure.¹⁹³ In recent years, fabrication of In_2O_3 has received much interest, such as luminescent spectra peaking at 480 and 520 nm from In_2O_3 nanoparticles reported by Zhou *et al.*,¹⁹⁴ 450 nm from In_2O_3 nanocubes¹⁹⁵ and 378, 398, and 420 nm from In_2O_3 nanofibers reported by Qian *et al.*¹⁹⁶ The emission from oxide semiconductors is mainly attributed to the oxygen vacancies. In addition, Yang *et al.*¹⁹⁷ have well investigated the synthesis and luminescent properties of the In_2O_3 nano/micro-structures with two different morphologies (nanorod bundles and caddice sphere-like agglomerates). In_2O_3 nanorod bundles and spheres showed similar blue emission peaking around 416 and 439 nm under 383 nm UV excitation. Moreover, Fang *et al.*¹⁹⁸ also reported highly uniform and quasi-monodisperse In_2O_3 nanocrystals, which gave a relatively strong emission centered at 423 nm and a shoulder located at about 392 nm with weak quantum confinement effects at room temperature. All the research work suggests that the indium oxide is also an important alternative defect-related luminescent material. According to the existing investigations, in summary, some low-toxic and wide-band-gap semiconductor oxides can potentially be used as efficient and defect-related luminescent materials. Detailed information and representative research is listed in Table 3.

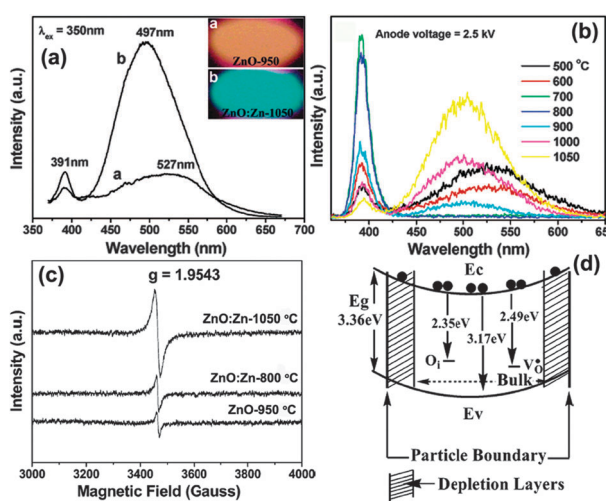


Fig. 10 (a) PL spectra (inset: photographs under irradiation of a 365 nm UV lamp), (b) CL spectra, and (c) EPR curves of ZnO-based phosphors. (d) Schematic diagram of the energy band of a ZnO-based particle in cross section (Ec: conduction band, Ev: valence band, Eg: band gap) (reproduced with permission from ref. 176, copyright 2006, American Chemical Society).

3.4. BCNO phosphors

Recently, oxynitride and nitride compounds have emerged as promising environmentally friendly phosphor candidates because of their excellent properties of non-toxicity, outstanding thermal

and chemical stability, and high luminescence efficiency.^{26,199} In previous work, BCN compounds were expected to behave as semiconductors with bandgap energies that could be tunable by varying the atomic composition. Therefore, this kind of materials was considered to be intermediate between graphite and hexagonal-BN (h-BN).²⁰⁰ However, it was very difficult to improve the light-emitting properties of this BCN phosphor, which had only single emission peaks in the PL and showed low PL intensity and quantum efficiency. Most recently, Okuyama and co-workers reported a simple and useful synthetic route for BCNO phosphor with high quantum efficiency (as high as 79%) and wavelength-tunable emission ranging from 387 to 571 nm.^{26,199,201–203} The experimental results indicated that this phosphor was polycrystalline in nature and composed of several distinct nanocrystals. Moreover, higher PL intensity and quantum efficiency have been achieved by controlling the carbon content, PEG/B ratio in the precursor solution, and reaction time during the preparation of BCNO phosphors (Fig. 11A).¹⁹⁹ This result showed that carbon atom impurities were able to substitute for boron or nitrogen atoms in the *t*-BN crystallites with increased carbon concentration. As a result, the allowed electronic transitions in the matrix were modified and the states generated by carbon were changed, that is to say the variations of the BCNO band gap results from changes in the chemical composition of the BCNO crystals. Furthermore, the variations of band gap can cause shifts of their emission spectra and different emission colors.^{199,201–203}

Another research group of Qiu *et al.* also fabricated BCNO-based phosphors and well investigated their photoluminescence properties.²⁰⁴ Some of their research work focused on BCNO-nanoparticle-embedded polymer electrospun nanofibers prepared by an electrospinning technique. These nanofibers showed a wide band emission in the visible region, which originated from the defect-related BCNO nanocrystals and can be changed by adjusting the C content during the preparation of BCNO phosphors. In addition, they also assumed the paramagnetic defect centre originated from electrons trapped at nitrogen vacancies, and this defect was responsible for the observed luminescence of the BCNO nanocrystals.²⁰⁴ In a further study, Qiu and co-workers also reported a BCNO-based long-persistence phosphor,^{205,206} which shows a phosphorescence peak centered at 520 nm. Its afterglow decay curve fitting $t^{-0.93}$ indicated a relatively slow decay rate (Fig. 11B). Moreover, they pointed out that this defect-related long-persistence luminescent BCNO phosphor was competitive as a commercial long-persistence phosphor (*e.g.*, SrAl₂O₄:Eu²⁺, Dy³⁺)²⁰⁷ for application in many fields due to its excellent luminescent properties, low cost, and low toxicity.

3.5. Titanates

ATiO₃ (A = Ca, Sr, Ba, Pd, *etc.*)-type perovskites, which have an energy band gap of about 3.0 eV, have recently attracted a good deal of attention due to their ferroelectric and electro-optical properties.^{208–211} Pizani *et al.* reported a series of disordered (amorphous) BaTiO₃, PbTiO₃, and SrTiO₃ materials prepared by a sol-gel method.⁹¹ These three materials displayed a similar broad emission band in the visible region under UV

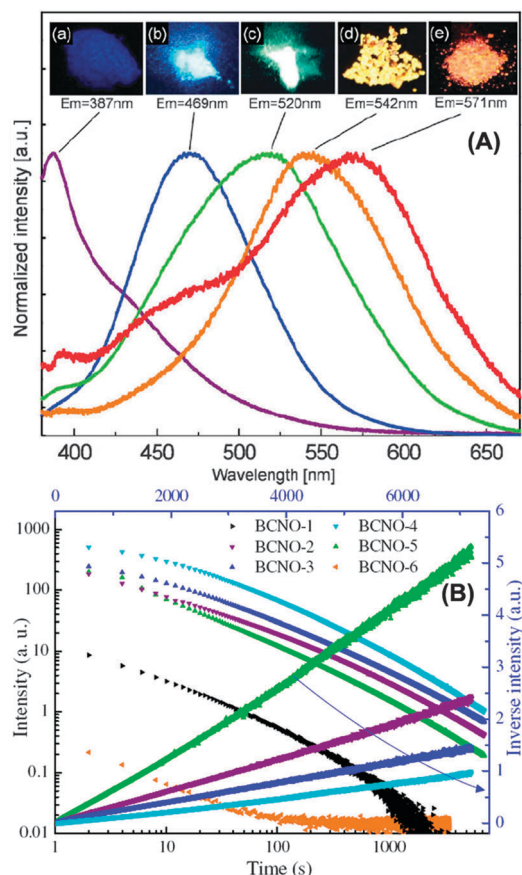


Fig. 11 (A) Photographs and corresponding emission spectra excited at 365 nm of BCNO samples prepared under various conditions of PRG/B ratio, temperature, and heating time [(a) 2.0×10^{-3} , 900 °C, 30 min; (b) 2.0×10^{-3} , 800 °C, 30 min; (c) 4.0×10^{-3} , 700 °C, 60 min; (d) 4.0×10^{-3} , 700 °C, 45 min; (e) 4.4×10^{-3} , 700 °C, 30 min] (reproduced with permission from ref. 199, copyright 2008, Wiley). (B) Afterglow decays of BCNO-1 to BCNO-6 recorded at the respective peaking wavelength after termination of irradiation with an UV lamp for 10 min (starting materials with fixed atomic ratios of B/C = 2/3 and B/N = 1/7, 1/6, 1/5, 1/4, 1/3 for BCNO-1 to BCNO-5, and B/C = 1/2, B/N = 1/3 for BCNO-6, respectively) (reproduced with permission from ref. 206, copyright 2009, IOP Science).

excitation. The origin of the photoluminescence was not exactly identified. However, the experimental results indicated that it could be related to the disordered perovskite structure. In addition, they also synthesized amorphous luminescent PbTiO₃ thin films.⁹² Lazaro and co-workers produced ordered-disordered CaTiO₃ with photoluminescence prepared by a polymeric precursor method and annealed at 450–600 °C for 2 h.²¹² The authors proposed that this photoluminescence in CaTiO₃ was affected not only by disorder in the lattice former but also by structural disorder in the lattice modifier. Pontes *et al.* also reported the role of network modifiers in the creation of photoluminescence in CaTiO₃.²¹³

Takahashi *et al.* produced orange luminescent barium titanate silicate BaTiSi₂O₇ by a conventional solid-state reaction.²¹⁴ This product displayed visible orange luminescence. Correspondingly, the broad PL emission with a peak at 580 nm was observed by ultraviolet excitation at 321 nm. The authors further suggested that this luminescence property was related

to both the absolutely isolated pyramidal TiO_5 unit pair and the oxygen defect in the TiO_5 unit in the $\text{BaTiSi}_2\text{O}_7$ phase. Besides the above-mentioned titanates, a strong blue emission band at 480 nm has been observed in nano-sized $\text{La}_{0.5}\text{Na}_{0.5}\text{TiO}_3$, reported by Zhang.²¹⁵ In this report, the emission band is closely related to the electron transitions between the conduction band and the defect levels, between the defect levels and valence band, as well as between the defect levels. Interestingly, a emission pattern very similar to that of ATiO_3 was also observed, and the independence of the emission band on the preparation method of the material was revealed.

3.6. Fluoride materials

Fluoride materials have been studied for a very long time because they have a wide range of potential optical applications based on their low energy phonons and high ionicity.²¹⁶ In the past few years, our group has successfully synthesized well-dispersed fluoride nanocrystals, including alkaline earth metal fluorides (CaF_2 , SrF_2 , BaF_2)⁹⁷ and $\text{KRE}_3\text{F}_{10}$ ($\text{RE} = \text{Sm-Lu, Y}$).¹¹⁰ These as-obtained fluoride nanocrystals can show a strong emission band with maximum at 400 nm under UV excitation.⁹⁷ Since we did not introduce any other activated ions in the experiments, the emission has to be caused by some kind of defect or electronic centre. In addition, we also observed that the lifetimes of these three fluoride nanocrystals are 7.6 ns (CaF_2), 8.4 ns (SrF_2) and 17.4 ns (BaF_2), respectively. The short lifetimes further proved that their luminescence originated from defects or electronic centres in the fluoride nanocrystals. These defect emission centers may be induced by the adsorbed oleic acid molecules onto the surfaces of the nanocrystals in the formation process. Similarly, the as-prepared well-dispersed $\text{KRE}_3\text{F}_{10}$ ($\text{RE} = \text{Sm-Lu, Y}$) nanocrystals also displayed self-activated luminescence due to the trap states of surface defects.¹¹⁰

3.7. Carbon nanomaterials

3.7.1. Carbon nanodots. Recently, emerging light-emitting quantum-sized (less than 10 nm) carbon nanodots (CNDs) have appeared to be a promising alternative to traditional luminescent materials in many applications because of their advantages in size, biocompatibility, low toxicity, and cheaper cost.²⁹ The synthesis of the CNDs can be generally classified into two kinds of approaches. Firstly, CNDs can be obtained from a larger structure (Fig. 12a), such as graphite,²¹⁷ carbon nanotubes,²¹⁸ and so on.²¹⁹ In the other kind of strategy, CNDs are prepared from some organic molecular precursors.^{220–223} Generally, during these methods, CNDs often undergo oxidation (such as HNO_3 and/or H_2SO_4) and further purification processes. Therefore, CNDs typically contain many functional groups (such as carboxylic and hydroxyl groups) on the surface (Fig. 12b), thus imparting them with excellent water solubility and suitability for subsequent functionalization with various organic, polymeric, inorganic, or biological species. For the physical and chemical properties of CNDs, Ray *et al.*²²⁴ reported that CNDs formed from oxidation of candle soot consisted of a nanocrystalline core of graphitic sp^2 carbon atoms functionalized with peripheral carboxylic/carbonyl moieties. Another research group demonstrated that Raman

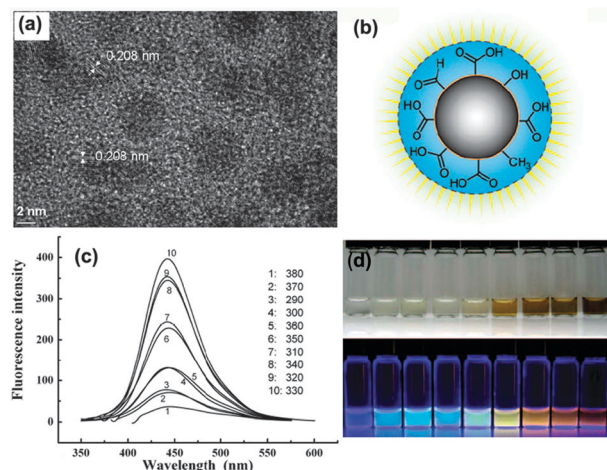


Fig. 12 (a) Representative TEM micrographs of CNDs (reproduced with permission from ref. 225, copyright 2009, American Chemical Society). (b) Depiction of CNDs after surface oxidative treatment (reproduced with permission from ref. 29, copyright 2010, Wiley). (c) PL emission spectra of 1.9 nm CNDs at different excitation wavelengths of 290–380 nm (reproduced with permission from ref. 226, copyright 2008, Royal Society of Chemistry). (d) Optical images of polyacrylamide gel electrophoresis (PAGE)-separated CNDs illuminated under white (top) and UV light (312 nm; center) (reproduced with permission from ref. 227, copyright 2007, Wiley).

spectra of CNDs that were produced by electrochemical oxidation of nanotubes showed characteristics of both sp^2 and disordered carbon.²¹⁸ Based on further and detailed study, CNDs consist of an amorphous to nanocrystalline core with predominantly sp^2 carbon and the lattice spacings are consistent with graphitic or turbostratic carbon.^{223,225,226}

Typically, CNDs can show strong optical absorption in the UV region and even the visible range, which depends on the synthesis method and surface modification.²¹⁷ However, the most fascinating features of CNDs are the photoluminescence properties. The emission spectra of CNDs prepared by Chen and co-workers have a broad color range with the maximum at the range of 415–615 nm.²²⁵ Ray *et al.* reported fluorescent carbon nanoparticles with a size of 2–6 nm which can be prepared by oxidation of soot particles. Surface oxidation and subsequent nitrogen/oxygen doping afforded a light emission property of the carbon particles. The luminescence of carbon particles depends on the wavelength of excitation light and the particle size, that is, the smaller the size, the higher the luminescence efficiency.²²⁴ In general, the emission intensities and the color can be influenced by the synthesis methods, different excitation wavelengths (Fig. 12c), particle size (Fig. 12d), surface properties of the CNDs themselves,^{219,225,226} and other external factors (such as ionic strength and pH values).^{221,227} Since the elemental carbon itself is nonluminous and has no extrinsic activators, the observed luminescence from CNDs must be related to some defects and/or impurities in the system. Due to its complexity and difficulty, the exact mechanism is still a matter of current debate and requires further investigation. However, based on the research results, besides the quantum effect of the CNDs, the carbon-based photoluminescence has been attributed by many researchers to passivated defects on the carbon particle surface acting as excitation energy traps.^{217,218}

Additionally, the performance in an *in vivo* study using CD-1 mice suggests the nontoxicity of CNDs at exposure levels and times beyond those typically used for optical *in vivo* imaging studies.²²⁸

3.7.2. Graphene oxide. Graphene oxide (GO) is an atomically thin sheet of graphite, and is increasingly attracting chemists for its characteristics. Graphene oxide contains oxygen-containing functional groups on the surface, such as carboxylic and hydroxy groups, thus imparting it with excellent water solubility, suitability, and a mixture of sp^2 - and sp^3 -hybridized carbon atoms, which may provide interesting possibilities for optical applications.²⁹

In 2008, Dai and co-workers^{229,230} reported intrinsic fluorescence in both the visible and the near-infrared (NIR) regions from nanosized GO functionalized with PEG. Owing to its small size, intrinsic optical properties, large specific surface area, low cost, and low toxicity, GO as a promising new material has attracted much attention in the following studies.^{231–234} Chhowalla and co-workers reported near-UV-to-blue photoluminescence from solution-processed graphene oxide. Moreover, they presumed that the PL of this kind of GO originated from the recombination of electron–hole (e–h) pairs, localized within small sp^2 carbon clusters embedded within the sp^3 matrix.²³⁵ The PL behavior of GO is very similar to that observed in CNDs.²⁹ Therefore, both GO and CNDs may become promising platforms that pave the way toward interesting biomedical labeling and optoelectronics applications.

3.8. Inorganic–organic hybrids

Other attractive species of defect-related luminescent materials include inorganic–organic hybrids with advanced optical properties, such as high laser efficiencies, good photostability, photopattern waveguiding structures for integrated optics, electroluminescent diodes, and so on.^{23–25,236–238} Carlos and co-workers have paid much attention on the hybrid concept to synthesize stable and efficient photoluminescent materials lacking metal activator ions, such as urea cross-linked inorganic–organic hybrids (so-called ureasils), amine-functionalized inorganic–organic hybrids, and urea/urethane cross-linked nanohybrids prepared by a sol–gel method at room temperature.^{239,240} Generally, the host matrix of this kind of hybrid material is a silica-based network and covalently grafted by means of urea, urethane, or amido-group linkages. Controlling the experimental conditions and excitation energy, the inorganic–organic hybrids can show tunable photoluminescence, and even efficient white-light hybrids with high photoluminescence yield. Moreover, Carlos *et al.* proposed a mechanism based on NH_3^+/NH^- (or NH_2^+/N^-) donor–acceptor pairs to explain the emission of these materials.²³ Similarly, Lianos *et al.* prepared hybrid inorganic–organic nanoclusters. These inorganic–organic hybrids were founded on a silica backbone but they were also facilitated and assisted by forces arising from hydrophilic/hydrophobic balance and hydrogen-bonding interactions. Luminescence was attributed to electron–hole recombination on delocalized states so that emission wavelength can be tuned in the range of almost the entire visible spectrum by choosing the excitation wavelength.¹⁹

In a recent study, Guo *et al.* discovered the white-light-emitting borate-based inorganic–organic hybrid open framework.²⁴¹

The two three-dimensional (3D) inorganic–organic hybrid isopolyacid borates, $B_6O_9(en)$ and $(H_2en)_2(Hen)_2B_{16}O_{27}$ (*en* = ethylenediamine) were first prepared under solvothermal conditions. Especially, the $(H_2en)_2(Hen)_2B_{16}O_{27}$ hybrid can show bright luminescence and be modified from blue to white by means of a simple heat-treatment process. Since no metal activator ions exist in this compound, the self-activating photoluminescence probably originates from structural defects caused by heat treatment. This is supported by the τ_f value at ns level and the results of the PL spectra, suggesting its fluorescence character. In addition, they also pointed that the compound of $(H_2en)_2(Hen)_2B_{16}O_{27}$ with large void spaces may find utility in ion exchange in the future.

4. Emission mechanisms

To date, researchers have extensively investigated defect-related phosphors, however the origins of luminescence are not yet entirely understood in defect-related materials. Unlike emission from rare earth activator-doped luminescent materials, it is difficult to confirm the kinds of defects that cause emission and how it works in the matrix. A variety of possible mechanisms have been proposed. According to the existing investigations, we grouped the defect-related luminescent mechanisms into four systems, which have some special characters, and can be summarized as follows:

(i) Carbon impurities (defects)

Carbon defects are only luminescently active after heat treatment, because these samples are not luminescent prior to this procedure. These carbon-related defect centers include an electron being localized in a 2p orbital of a single-bonded carbon and single-bonded oxygen. This would give rise to photoluminescence through a strong electron–photon coupling.^{43,112} Generally, the luminescence from carbon defects contains several common features, such as characteristic emission range (350–700 nm), maximum of emission spectrum (405–550 nm) and shorter PL lifetime (less than 10 ns).^{17,43,86–88}

(ii) Oxygen vacancies

Oxygen vacancies are known to be one of the most common defects in oxides and usually act as radiative centers in luminescence processes.¹⁹¹ As the annealing process can cause recovery of the structural defects and eliminate efficiently the non-radiative combination centers, the oxygen vacancy-related photoluminescence is strongly dependent on the calcination temperature and time.¹⁷⁶ The recombination of a conduction band electron with an oxygen vacancy can yield visible emission. Moreover, each recombination luminescence includes the following processes: ionization, migration, recombination, and emission.^{87,88,176} This recombination process results in the long lifetime (μ s or ms).

(iii) E'-type luminescent centers

An E'-type luminescent center ($^*Si\equiv$) is an unpaired electron localized in a single Si sp^3 orbital (*i.e.* a silicon dangling bond), where the spin is highly localized on the silicon atom.¹⁵² This is a prominent paramagnetic defect in conventional a-SiO₂. This

defect can result in characteristic photoluminescence at about 288 nm when excited with high-energy photons.^{152,156}

(iv) Nonbridging oxygen hole centers

Nonbridging oxygen hole centers are intrinsic defect centers in amorphous and porous silica and can be described as $\text{SiOH} \rightarrow \text{SiO}^\bullet + \cdot\text{H}$, where dots represent unpaired electrons. In the PL spectra of silica-based systems, this defect was connected with bands at 1.8 and 1.9 eV.^{151–153} Unfortunately, the silanol groups (SiOH) are unstable when exposed to ambient air and oxidized slowly to form Si dangling bonds, which form non-radiative recombination centers and influence PL efficiency.

(v) Peroxy-radical hole trap

Peroxy-radical hole traps (PRHT, $\cdot\text{O}-\text{O}-\text{Si}\equiv\text{O}_3$) are also intrinsic defect sites in the silica lattice. This kind of defect consists of an unpaired electron localized over two oxygens, one of which is bonded to Si.³¹ Therefore, they can introduce an electronic state into the band gap, resulting in characteristic photoluminescence at about 460 nm (2.7 eV) when excited with high energy photons ($h\nu \geq 3.5$ eV or $\lambda \leq 357$ nm).⁸⁶

(vi) Carbon dioxide radical

Carbon dioxide radicals ($\text{CO}_2^\bullet-$) are a kind of paramagnetic defect resulting from bond cleavages of some organic additives during the synthesis process.^{90,103–106} These radicals are trapped into the matrix lattice or interstitial positions, which are apparently the precursors for various centers. These defect centers induce an electron localized in the 2p orbital of the single-bonded carbon. This would give rise to photoluminescence with a short lifetime through strong electron–photon coupling.

(vii) Donor–acceptor pairs

Donor–acceptor pairs (such as $\text{NH}_3^+/\text{NH}^-$ or NH_2^+/N^-) can usually be found in room temperature-obtained organic/inorganic hybrids. This mechanism was proposed by Carlos *et al.*^{23,239,240} Photoinduced proton-transfer between defects such as NH_3^+ and NH^- or NH_2^+ and N^- can give rise to photoluminescence. This process is a shorter-lived electron–hole recombination occurring in organic/inorganic hybrids. Similarly, radiative recombination of electron–hole pairs in carbon nanomaterials (*i.e.* graphene) can also lead to fluorescence.³⁰ The characteristic luminescent properties are a broad emission band, a short lifetime, and tunable emission color.

5. Potential applications

5.1. Lighting

Because of the great interest in the generation of white-light emission for a variety of applications (such as solid-state multicolor three-dimensional displays, back lighting, *etc.*), researchers have paid much attention in this field.^{242–244} At present, the most commonly used white-light source is white light-emitting diodes (LEDs),^{245,246} which is a GaN blue LED encapsulated with a yellow-emitting phosphor coating (commercial YAG:Ce³⁺ phosphors, which are expensive and require high production temperatures).²⁴⁷ Because of the exceptional performance characteristics (*e.g.* low cost and non-toxicity), a

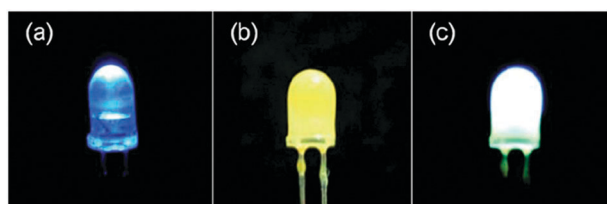


Fig. 13 An example application of BCNO phosphors in white LEDs. (a) A 5 mm reference GaN/SiC LED chip illuminating blue light, (b) the same LED chip coated with a thin layer of the BCNO sample prepared at 700 °C after treatment with a polymer solution, and (c) upon illumination, the same LED shows a bright white light (reproduced with permission from ref. 26 and 203, copyright 2009, Royal Society of Chemistry and ECS The Electrochemical Society).

novel yellow-emitting defect-related BCNO phosphor has been used in a white LED by Okuyama's group.^{28,213} In their study, defect-related BCNO phosphor particles were coated on the surface of a commercial blue GaN/SiC LED chip. Bright white-light emission was achieved when it was excited by the blue emission from the GaN/SiC chip (Fig. 13). Therefore, it can be inferred that the environmentally-friendly and low cost defect-related luminescent materials may find potential applications in the field of white LEDs.

On the other hand, white light-emitting devices with multiple emitting components, which are generally rather complicated and expensive, can be problematic as it is difficult to control the color balance. For this reason, one current academic interest in white light is pursuing single white light-emitting phosphors to avoid the intrinsic color-balance, device-complication, and high-cost problems.^{241,248–251} Due to the excellent blue emission of defect-related apatite structure phosphors described above, it may be an attractive alternative to commercially blue phosphors. In further study, our group induced Ce³⁺ and Mn²⁺ to defect-related FAP nanorods and obtained the FAP:Ce³⁺, Mn²⁺ samples with multicolor emission, which consists of an ultraviolet emission centered at 357 nm attributed to the 5d–4f transition of Ce³⁺, a radical-related blue emission band ranging from 360 to 500 nm, and a yellow emission centered at 561 nm from the ${}^4\text{T}_1 \rightarrow {}^6\text{A}_1$ transition of Mn²⁺.¹⁰⁵ Moreover, with increase of the excitation wavelength from 295 to 342 nm, the PL intensities of ultraviolet and yellow emissions decrease, and the blue emission increases (Fig. 14). The change in relative intensities of these three color parts can result in tunable luminescence from blue to white to yellow for these samples. Especially, when adjusting the excitation light to 308 nm, the blue and yellow emissions are comparable in intensity to give white-light emission. The corresponding chromaticity coordinate for this white light excited by 308 nm is calculated to be $x = 0.316$ and $y = 0.328$, which is very close to the standard equal energy of ideal white-light illumination ($x = 0.333$ and $y = 0.333$) according to the 1931 CIE coordinate diagram. Similarly, in order to improve the emission in the red-light range, Guo and co-workers introduced Eu³⁺ ions into a borate-based inorganic–organic hybrid open framework by soaking it in an aqueous solution of EuCl₃,²⁴¹ resulting in a white light-emitting hybrid sample. This novel strategy of combining defect-related luminescence and metal-activator emissions might serve as guidance for the design and fabrication of other

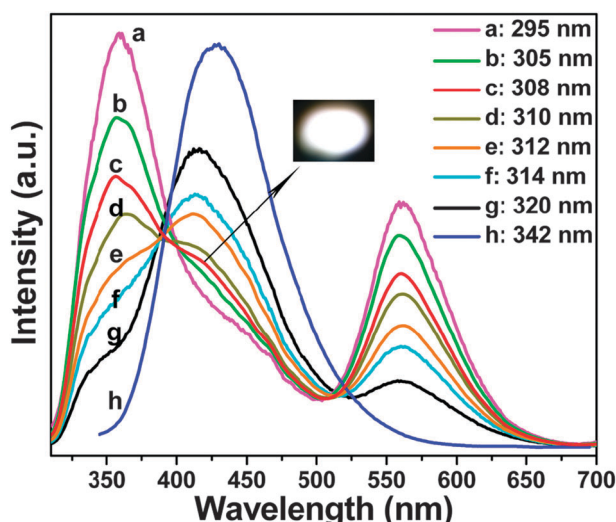


Fig. 14 PL emission spectra for as-synthesized FAP:Ce³⁺, Mn²⁺ sample under different excitation wavelengths: (a) 295, (b) 305, (c) 308, (d) 310, (e) 312, (f) 314, (g) 320, (h) 342 nm. The inset shows the corresponding luminescence photograph for the sample under excitation at 308 nm (reproduced with permission from ref. 105, copyright 2010, Royal Society of Chemistry).

materials with white-light emission and tunable luminescent properties.

5.2. Application in biomedical fields

Luminescent materials including fluorescent organic molecules²⁵² and semiconductor nanoparticles²⁵³ have been widely investigated in biomedical areas. However, some serious problems of photo-bleaching and quenching of fluorescent organic molecules and the toxicity of semiconductor quantum dots are critically

pronounced, which have seriously limited their applications in biomedical areas. Because of the excellent characteristics of low cost and non-toxicity, the defect-related luminescent materials have great potential in medical applications.

5.2.1. Drug delivery. An ideal drug-delivery system should possess several important properties, which are biocompatibility, nontoxicity, proper particle size, and the ability to transport the desired drug molecules to the targeted cells or tissues and release in a controlled manner.^{254–257} So far, different types of drug-delivery systems have been developed.²⁵⁴ Among them, mesoporous nanomaterials have gained enhanced interest with particular attention as drug storage and release hosts due to their unique surface and textural properties.^{255,258–261} Recently, our group has paid much attention to luminescent nanomaterials for biomedical application as drug delivery systems. We designed and synthesized the multifunctional SrHAp nanorods with mesoporous and defect-related luminescence by a simple hydrothermal process.¹⁰⁶ The experimental process, loading and release of drug molecules are presented in Fig. 15A. During the synthesis process, CTAB was selected as the organic template for the mesoporous structure of multifunctional SrHAp and removed through refluxing in acetone to form a mesoporous structure with mesopore size of 3–5 nm. Drug storage/release tests suggest that the multifunctional SrHAp nanorods show high drug loading and a controlled release property for ibuprofen (IBU) (Fig. 15B). Although the mesoporous SrHAp sample also exhibited blue emission (Fig. 15Cg) even after loading the drug molecules (Fig. 15Ca), the IBU-SrHAp sample (Fig. 15Ca) has a lower PL intensity than SrHAp (Fig. 15Cg). Moreover, the PL emission intensities of the multifunctional drug carriers increase with the amount of IBU released (Fig. 15C). Therefore, this

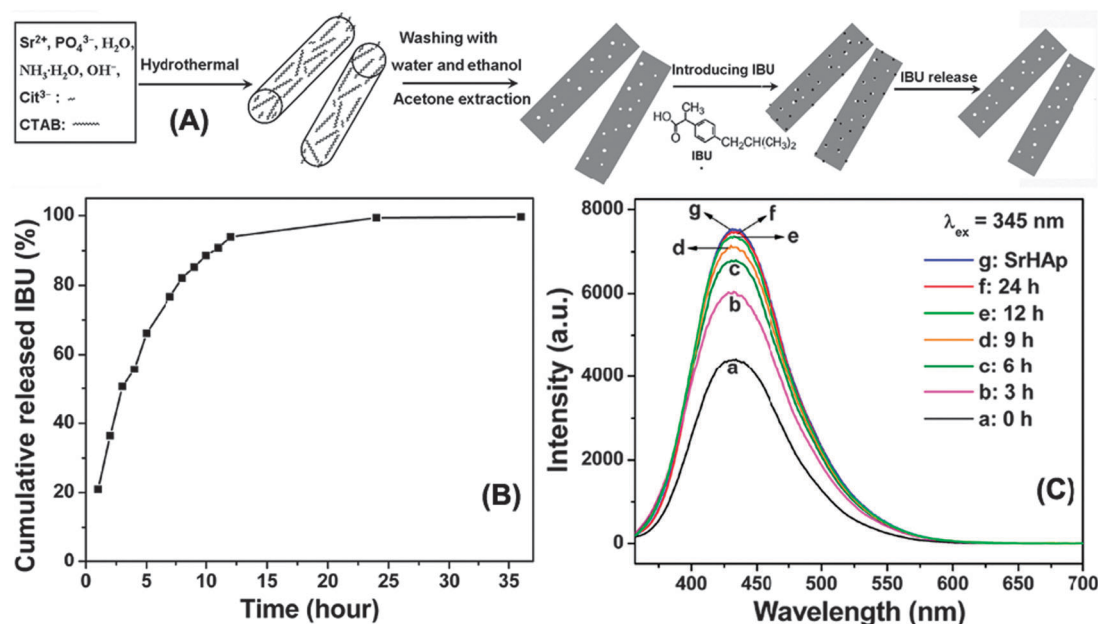


Fig. 15 (A) Schematic for the experimental process for luminescence mesostructure of SrHAp nanorods and subsequent loading and release of IBU. (B) Cumulative ibuprofen release from IBU-SrHAp system as a function of release time in the release media of the simulated body fluid (SBF) system. (C) PL emission spectra of IBU-SrHAp nanorods at different release time (reproduced with permission from ref. 106, copyright 2010, Elsevier).

relationship between the luminescence properties and drug release has potential as a probe for monitoring and tracking the drug release during the drug-release process.

In a follow-up study, to improve the mesoporous property, the design of multifunctional composite materials combining the mesoporous textures (MCM-48), spherical shape, and defect-related fluorescence were also prepared.⁹⁰ In this study, defect-related luminescent apatite was deposited on the surface and/or in the pores of the bioactive, mesoporous, and amorphous MCM-48 network, resulting in a higher drug loading system (33.7 wt%). In addition, defect-related luminescent porous silica fibers as drug carriers were also prepared and investigated due to many advantages, such as stable porous structure, tunable pore size, high specific surface area with abundant Si-OH active bonds on the pore walls, nontoxic nature, and good biocompatibility.¹²⁹

Shi *et al.* reported oxygen-deficient luminescent mesoporous silica nanoparticles with uniform morphology, size, and integrated mesoporosity–luminescent properties, which were synthesized by a bottom-up self-assembly route followed by a calcination process.²⁶² They also developed the biological applications of these functional nanoparticles for synchronous drug delivery and imaging.

Owing to the nano-size, intrinsic PL properties, and large specific surface area, GO is another promising new material for medical applications. The PEG-modified GO was exploited as a vehicle by Dai and co-workers for the antibody-targeted delivery of the widely used chemotherapy drug doxorubicin (DOX), which was loaded onto the GO-PEG surface by simple π -stacking-mediated physisorption.²²⁹ All these research reports

indicate that defect-related luminescent nanomaterials have good application prospects in the biomedical field of drug delivery.

5.2.2. Bioimaging. Fluorescence imaging is a very important technique for biological studies and clinical applications. Quantum dots and related core–shell nanoparticles (such as CdSe, NaGdF₄:Yb³⁺, Er³⁺/NaGdF₄ core–shell upconversion luminescent nanoparticles, and so on) have been used in various *in vitro* and *in vivo* optical imaging experiments.^{263–267} However, since heavy metals and/or rare earth ions are the essential elements of these two kinds of luminescent nanoparticles, they have prompted serious health and environmental concerns.²⁶⁴ Therefore, the search for benign alternatives has become increasingly important and urgent. With characteristics of tunable PL properties and low toxicity, defect-related luminescent nanomaterials form an attractive alternative for bioimaging applications.

Sun *et al.* have studied carbon dots for multiphoton bioimaging.²⁶⁸ First, they prepared nanosized carbon particles (sub-10 nm) with surface passivation by poly(propionylethylenimine-co-ethylenimine) (PPEI-EI). These kinds of CNDs can show strong luminescence with two-photon excitation in the near-infrared area, which has been attributed to passivated defects on the carbon particle surface acting as excitation energy traps.²¹⁷ Then, after incubation with CNDs for 2 h in an aqueous buffer at 37 °C followed by washing to remove any extracellular CNDs, the MCF-7 cells exhibited bright luminescence in both the cell membrane and cytoplasm regions when imaged on the fluorescence microscope with excitation by 800 nm laser pulses (Fig. 16a–c). Furthermore, the translocation of the CNDs

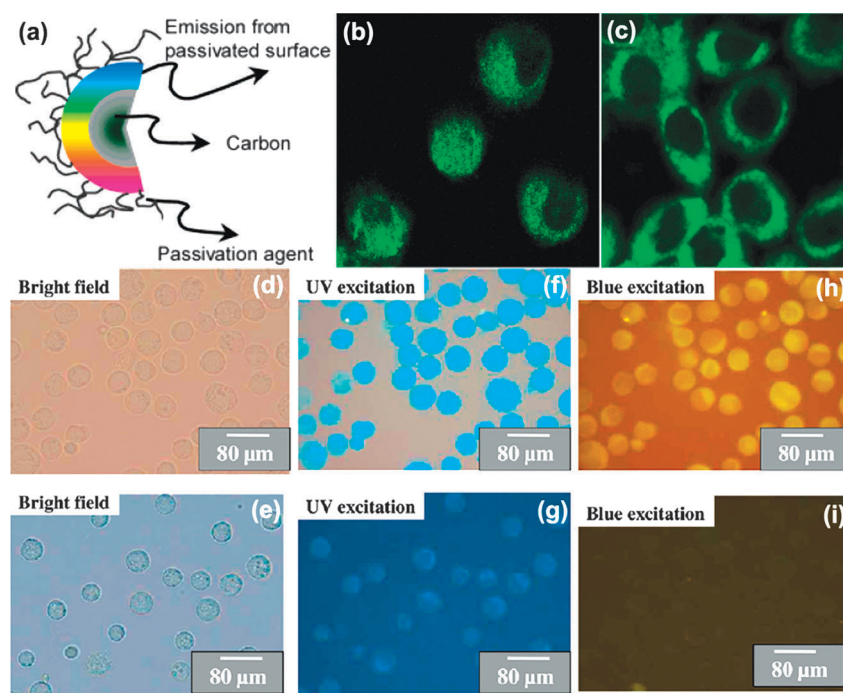


Fig. 16 (a) Schematic for the CND structure prepared by Sun *et al.* and (b, c) two-photon luminescence image (800 nm excitation) of human breast cancer MCF-7 cells with internalized CNDs passivated with PPEI-EI (reproduced with permission from ref. 268, copyright 2007, American Chemical Society). (d–i) Fluorescent CND-labeled EAC cells. Washed cells were imaged under bright field, UV, and blue light excitation. The bottom row images correspond to the control experiment where no CNDs were used. Cells become bright blue–green under UV excitation and yellow under blue excitation but were colorless in the control sample. The light blue color of the control sample under UV excitation is due to the well-known autofluorescence of cells (reproduced with permission from ref. 224, copyright 2009, American Chemical Society).

from outside the cell membrane into the cytoplasm is temperature dependent, and no meaningful CND internalization was observed at 4 °C. These results indicate that the luminescent CNDs can be potentially used for cell imaging with two-photon luminescence microscopy.

Additionally, many other studies on the bioimaging capabilities of CNDs have followed Sun *et al.*'s work.^{217,228,268,269} Among them, Ray and co-workers reported fluorescent carbon nanoparticles (2–6 nm) with excellent water solubility used for conventional bioimaging.²²⁴ In this study, a CND solution was mixed with cell culture media along with Ehrlich ascites carcinoma cells (EACs), incubated for 30 min, and then the cells were washed. These labeled cells can show a bright blue-green color under UV excitation and yellow under blue excitation, but they are colorless in the control sample without CNDs (Fig. 16d–i). This result demonstrates that CNDs can enter into the cells without any further functionalization and the CND-labeled cells show encouraging cell-imaging applications using a conventional fluorescence microscope. Some other researchers also predict that the biocompatibility of CNDs may be competitive with some currently FDA-approved dyes used as optical imaging agents such as indocyanine green ($LD_{50} = 60 \text{ mg kg}^{-1}$ body weight).²²⁸ Similarly, luminescent GO is also an excellent alternative in bioimaging applications because of its advantages in size, biocompatibility, and low toxicity.^{229,230}

6. Summary and outlook

Defect-related luminescent materials are interesting newcomers to the world of phosphors. In the past decade, the development of novel defect-related phosphors has greatly accelerated due to the emphasis on environment/health and the combination of nanotechnology and biology. In this review, we have discussed the importance of metal-activator-free phosphors and their unique luminescent properties for technological advances. We have also outlined the common strategies for the synthesis of defect-related luminescent materials using inexpensive raw materials with control over compositions, sizes, and shapes, and their applications in lighting and biology. The novel defect-related phosphors exhibit tunable color emission within the violet-to-red range and even near-infrared with high efficiency and stability, which can also be excited by a wide range of light, ranging from short UV (254 nm) to blue light. In addition, long-duration phosphorescence was observed in these kinds of phosphors. The defect-related phosphors stand to have a huge effect on both health and environmental applications due to their potential to serve as low-/nontoxic replacements to toxic traditional heavy-metal- or rare earth-ion-based luminescent materials. Although substantial and rapid progress has been made in the synthesis, properties, and applications of defect-related phosphors in the recent years, developing better synthetic routes and more detailed fundamental studies of their properties have a level of urgency, as there still remains much room for improvement in the coming years. First, despite the fact that there are many kinds of possible luminescent mechanisms proposed by researchers, further and detailed investigations are still required to explore exactly how the defects work, and

to develop better synthesis routes to these emerging materials. Secondly, as these kinds of phosphors are related to defects/impurities in the matrix, how to precisely control the content and species of defects in the matrix is also a difficult issue to be addressed. Thirdly, although the photoluminescence has been extensively investigated by many researchers, basic studies of electroluminescence and cathodoluminescence properties of defect-related phosphors should be carried out for various electronics-related applications. Finally, to move forward, researchers with various backgrounds may be needed to develop strategies to further tune the properties and applications of defect-related environmentally-friendly phosphors. One key area will be the integration of defect-related phosphors with organic molecules or special characteristics (such as magnetization) to open the door to novel multifunctional applications, for example magnetic resonance imaging (MRI). On the other hand, from the point of view of devices, fluorescence from defect-related phosphors over a wide range of wavelengths (emission in the violet-to-red region, and even the near-infrared region) might offer possibilities for incorporation in solar photovoltaic conversion, sensors (*i.e.* electrochemiluminescence sensors, fluorescent sensors, *etc.*), field emission displays, optical information transmission, and display applications on flexible platforms.

Acknowledgements

This project is financially supported by National Basic Research Program of China (Grant No. 2010CB327704), National High Technology Program of China (2011AA03A407), the National Natural Science Foundation of China (Grant Nos. NSFC 50872131, 51172228, 21101149, 51172227, 20921002), and Science Foundation for Excellent Youth Scholars of Hebei Education Department (Grant No. Y2012007).

Notes and references

- 1 C. Feldmann, T. Jüstel, C. R. Ronda and P. J. Schmidt, *Adv. Funct. Mater.*, 2003, **13**, 511–516.
- 2 G. Blasse and B. C. Grabmaier, *Luminescent Materials*, Springer-Verlag, Berlin, 1994.
- 3 Y. Liu, D. Tu, H. Zhu, R. Li, W. Luo and X. Y. Chen, *Adv. Mater.*, 2011, **22**, 3266–3271.
- 4 V. P. Tuyen, T. Hayakawa, M. Nogami, J. R. Ducle and P. Thomas, *J. Solid State Chem.*, 2010, **183**, 2714–2719.
- 5 P. A. Tanner, Z. Pan, N. Rakov and G. S. Maciel, *J. Alloys Compd.*, 2006, **424**, 347–349.
- 6 W. C. Ke, C. C. Lin, R. S. Liu and M. C. Kuo, *J. Electrochem. Soc.*, 2010, **157**, J307–J309.
- 7 W. Luo, C. Fu, R. Li, Y. Liu, H. Zhu and X. Y. Chen, *Small*, 2011, **7**, 3046–3056.
- 8 L. X. Yu and M. Nogami, *Mater. Lett.*, 2010, **64**, 1644–1646.
- 9 C. H. Zheng, C. G. Hu, X. Y. Chen, H. Liu, Y. F. Xiong, J. Xu, B. Y. Wan and L. Y. Huang, *CrystEngComm*, 2010, **12**, 3277–3282.
- 10 R. C. Ropp, *Luminescence and the Solid State*, Elsevier, Amsterdam, Netherlands, 1991, vol. 12, p. 283.
- 11 Q. Y. Zhang and X. Y. Huang, *Prog. Mater. Sci.*, 2010, **55**, 353–427.
- 12 X. T. Zhang, T. Hayakawa, M. Nogami and Y. Ishikawa, *J. Alloys Compd.*, 2011, **509**, 2076–2080.
- 13 G. G. Li, D. M. Geng, M. M. Shang, C. Peng, Z. Y. Cheng and J. Lin, *J. Mater. Chem.*, 2011, **21**, 13334–13344.
- 14 G. G. Li, Z. Y. Hou, C. Peng, W. X. Wang, Z. Y. Cheng, C. X. Li, H. Z. Lian and J. Lin, *Adv. Funct. Mater.*, 2010, **20**, 3446–3456.

- 15 B. H. Lee, H. G. Jeong and K. S. Sohn, *J. Electrochem. Soc.*, 2010, **157**, J227–J232.
- 16 S. Angelov, R. Stoyanova, R. Dafinova and K. Kabasanov, *J. Phys. Chem. Solids*, 1986, **47**, 409–412.
- 17 W. H. Green, K. P. Le, J. Grey, T. T. Au and M. J. Sailor, *Science*, 1997, **276**, 1826–1828.
- 18 T. Hayakawa, A. Hiramitsu and M. Nogami, *Appl. Phys. Lett.*, 2003, **82**, 2975–2977.
- 19 T. Brankova, V. Bekiari and P. Lianos, *Chem. Mater.*, 2003, **15**, 1855–1859.
- 20 V. Bekiari and P. Lianos, *Langmuir*, 1998, **14**, 3459–3461.
- 21 V. Bekiari and P. Lianos, *Chem. Mater.*, 1998, **10**, 3777–3779.
- 22 B. E. Yold, *J. Non-Cryst. Solids*, 1992, **147–148**, 614–620.
- 23 L. D. Carlos, R. A. Sá Ferreira, R. N. Pereira, M. Assunção and V. de Z. Bermudez, *J. Phys. Chem. B*, 2004, **108**, 14924–14932.
- 24 L. Fu, R. A. Sá Ferreira, N. J.O. Silva, L. D. Carlos, V. de Z. Bermudez and J. Rocha, *Chem. Mater.*, 2004, **16**, 1507–1516.
- 25 L. D. Carlos, V. de Z. Bermudez, R. A. Sá Ferreira, L. Marques and M. Assuncão, *Chem. Mater.*, 1999, **11**, 581–588.
- 26 W. N. Wang, T. Ogi, Y. Kaihatsu, F. Iskandarc and K. Okuyama, *J. Mater. Chem.*, 2011, **21**, 5183–5189.
- 27 E. Cordoncillo, F. J. Guaita, P. Escribano, C. Philippe, B. Viana and C. Sanchez, *Opt. Mater. (Amsterdam)*, 2001, **18**, 309–320.
- 28 J. Lin and K. Baerner, *Mater. Lett.*, 2000, **46**, 86–92.
- 29 S. N. Baker and G. A. Baker, *Angew. Chem., Int. Ed.*, 2010, **49**, 6726–6744.
- 30 K. P. Loh, Q. Bao, G. Eda and M. Chhowalla, *Nat. Chem.*, 2010, **2**, 1015–1024.
- 31 M. E. Gimon-Kinsel, K. Groothuis and K. J. Balkus, Jr., *Microporous Mesoporous Mater.*, 1998, **20**, 67–76.
- 32 Y. C. Lee, Y. L. Liu, J. L. Shen, I. J. Hsu, P. W. Cheng, C. F. Cheng and C. H. Ko, *J. Non-Cryst. Solids*, 2004, **341**, 16–20.
- 33 S. Munekuni, T. Yamanaka, Y. Shimogaichi, K. Nagasawa and Y. Hama, *J. Appl. Phys.*, 1990, **68**, 1212–1217.
- 34 R. Costi, A. E. Saunders and U. Banin, *Angew. Chem., Int. Ed.*, 2010, **49**, 4878–4897.
- 35 Y. Yin, C. K. Erdonmez, A. Cabot, S. Hughes and A. P. Alivisatos, *Adv. Funct. Mater.*, 2006, **16**, 1389–1399.
- 36 R. Si, Y. W. Zhang, L. P. You and C. H. Yan, *Angew. Chem., Int. Ed.*, 2005, **44**, 3256–3260.
- 37 A. L. Pénard, T. Gacoin and J. P. Boilot, *Acc. Chem. Res.*, 2007, **40**, 895–902.
- 38 C. X. Li, J. Yang, P. P. Yang, H. Z. Lian and J. Lin, *Chem. Mater.*, 2008, **20**, 4317–4326.
- 39 P. A. Tanner, *J. Nanosci. Nanotechnol.*, 2005, **5**, 1455–1464.
- 40 C. K. Lin, Y. Y. Li, M. Yu, P. P. Yang and J. Lin, *Adv. Funct. Mater.*, 2007, **17**, 1459–1465.
- 41 S. Y. Seo, S. Lee, H. D. Park, N. Shin and K. S. Sohn, *J. Appl. Phys.*, 2002, **92**, 5248–5251.
- 42 G. F. Wang, Q. Peng and Y. D. Li, *Acc. Chem. Res.*, 2011, **44**, 322–332.
- 43 C. K. Lin, C. M. Zhang and J. Lin, *J. Phys. Chem. C*, 2007, **111**, 3300–3307.
- 44 J. Yang, C. X. Li, X. M. Zhang, Z. Quan, C. M. Zhang, H. Y. Li and J. Lin, *Chem.–Eur. J.*, 2008, **14**, 4336–4345.
- 45 F. Wang, Y. Han, C. S. Lim, Y. Lu, J. Wang, J. Xu, H. Chen, C. Zhang, M. Hong and X. Liu, *Nature*, 2010, **463**, 1061–1065.
- 46 Z. G. Yan and C. H. Yan, *J. Mater. Chem.*, 2008, **18**, 5046–5059.
- 47 D. Tu, L. Liu, Q. Ju, Y. Liu, H. Zhu, R. Li and X. Y. Chen, *Angew. Chem., Int. Ed.*, 2011, **50**, 6306–6310.
- 48 H. Chander, *Mater. Sci. Eng., R*, 2005, **49**, 113–155.
- 49 S. Choi, R. M. Dickson and J. Yu, *Chem. Soc. Rev.*, 2012, **41**, 1867–1891.
- 50 Z. H. Xu, C. X. Li, P. Ma, Z. Y. Hou, D. M. Yang, X. J. Kang and J. Lin, *Nanoscale*, 2011, **3**, 661–667.
- 51 S. L. Gai, P. P. Yang, C. X. Li, W. X. Wang, Y. L. Dai, N. Niu and J. Lin, *Adv. Funct. Mater.*, 2010, **20**, 1166–1172.
- 52 Q. Ju, W. Q. Luo, H. M. Zhu, Y. S. Lu, R. F. Li and X. Y. Chen, *J. Nanosci. Nanotechnol.*, 2011, **11**, 9478–9483.
- 53 R. Liu, D. Tu, Y. Liu, H. Zhu, R. Li, W. Zheng, E. Ma and X. Y. Chen, *Nanoscale*, 2012, **4**, 4485–4491.
- 54 Q. Ju, D. Tu, Y. Liu, R. Li, H. Zhu, J. Chen, Z. Chen, M. Huang and X. Y. Chen, *J. Am. Chem. Soc.*, 2012, **134**, 1323–1330.
- 55 P. P. Yang, L. L. Lu, Z. W. Quan, S. S. Huang and J. Lin, *Biomaterials*, 2008, **29**, 692–702.
- 56 P. P. Yang, Z. W. Quan, C. X. Li, X. J. Kang, H. Z. Lian and J. Lin, *Biomaterials*, 2008, **29**, 4341–4347.
- 57 J. L. Vivero-Escoto, R. C. Huxford-Phillips and W. B. Lin, *Chem. Soc. Rev.*, 2012, **41**, 2673–2685.
- 58 Q. Ju, D. Tu, Y. Liu, H. Zhu and X. Y. Chen, *Comb. Chem. High Throughput Screening*, 2012, **15**, 580–594.
- 59 H. Goessmann and C. Feldmann, *Angew. Chem., Int. Ed.*, 2010, **49**, 1362–1395.
- 60 J. Kim, H. S. Kim, N. Lee, T. Kim, H. Kim, T. Yu, I. C. Song, W. K. Moon and T. Hyeon, *Angew. Chem., Int. Ed.*, 2008, **47**, 8438–8441.
- 61 C. G. Wang, J. L. Chen, T. Talavage and J. Irudayraj, *Angew. Chem., Int. Ed.*, 2009, **48**, 2759–2763.
- 62 D. Shi, Y. Guo, Z. Dong, J. Lian, W. Wang, G. Liu, L. Wang and R. C. Ewing, *Adv. Mater.*, 2007, **19**, 4033–4037.
- 63 J. C. G. Bünzli, *Chem. Rev.*, 2010, **110**, 2729–2755.
- 64 C. Bouzigues, T. Gacoin and A. Alexandrou, *ACS Nano*, 2011, **5**, 8488–8505.
- 65 Y. L. Dai, C. M. Zhang, Z. Y. Cheng, P. Ma, C. X. Li, X. J. Kang, D. M. Yang and J. Lin, *Biomaterials*, 2012, **33**, 2583–2592.
- 66 Z. Y. Hou, C. X. Li, P. Ma, G. G. Li, Z. Y. Cheng, C. Peng, D. M. Yang, P. P. Yang and J. Lin, *Adv. Funct. Mater.*, 2011, **21**, 2356–2365.
- 67 Z. H. Xu, P. Ma, C. X. Li, Z. Y. Hou, X. F. Zhai, S. S. Huang and J. Lin, *Biomaterials*, 2011, **32**, 4161–4173.
- 68 Y. Ruan, Q. B. Xiao, W. Q. Luo, R. F. Li and X. Y. Chen, *Nanotechnology*, 2011, **22**, 275701.
- 69 X. Michalet, F. F. Pinaud, L. A. Bentolila, J. M. Tsay, S. Doose, J. J. Li, G. Sundaresan, A. M. Wu, S. S. Gambhir and S. Weiss, *Science*, 2005, **307**, 538–544.
- 70 I. L. Medintz, H. T. Uyeda, E. R. Goldman and H. Mattoussi, *Nat. Mater.*, 2005, **4**, 435–446.
- 71 P. P. Yang, Z. W. Quan, Z. Y. Hou, C. X. Li, X. J. Kang, Z. Y. Cheng and J. Lin, *Biomaterials*, 2009, **30**, 4786–4795.
- 72 R. Mout, D. F. Moyano, S. Rana and V. M. Rotello, *Chem. Soc. Rev.*, 2012, **41**, 2539–2544.
- 73 M. Liong, J. Lu, M. Kovochich, T. Xia, S. G. Ruehm, A. E. Nel, F. Tamanoi and J. I. Zink, *ACS Nano*, 2008, **2**, 889–896.
- 74 Y. H. Deng, D. W. Qi, C. H. Deng, X. M. Zhang and D. Y. Zhao, *J. Am. Chem. Soc.*, 2008, **130**, 28–29.
- 75 A. Aboshi, N. Kurumoto, T. Yamada and T. Uchino, *J. Phys. Chem. C*, 2007, **111**, 8483–8488.
- 76 G. Vaccaro, S. Agnello, G. Buscarino, M. Cannas and L. Vaccaro, *J. Non-Cryst. Solids*, 2011, **357**, 1941–1944.
- 77 L. Vaccaro, A. Morana, V. Radzig and M. Cannas, *J. Phys. Chem. C*, 2011, **115**, 19476–19481.
- 78 G. L. Davies, J. E. McCarthy, A. Rakovich and Y. K. Gun'ko, *J. Mater. Chem.*, 2012, **22**, 7358–7365.
- 79 J. Lin, M. Yu, C. K. Lin and X. M. Liu, *J. Phys. Chem. C*, 2007, **111**, 5835–5845.
- 80 B. Dunn and J. I. Zink, *Acc. Chem. Res.*, 2007, **40**, 729.
- 81 W. Q. Luo, C. Y. Fu, R. F. Li, Y. S. Liu, H. M. Zhu and X. Y. Chen, *Small*, 2011, **7**, 3046–3056.
- 82 I. I. Hinić, G. M. Stanić and Z. V. Popović, *J. Sol-Gel Sci. Technol.*, 1999, **14**, 281–289.
- 83 N. Chioldini, F. Meinardi, F. Morazzoni, A. Paleari and R. Scotti, *Appl. Phys. Lett.*, 2000, **76**, 3209–3211.
- 84 C. F. Song, M. K. Lü, P. Yang, F. Gu, D. Xu and D. R. Yuan, *Mater. Sci. Eng., B*, 2002, **94**, 181–185.
- 85 S. Fujihara and S. Kitta, *Chem. Phys. Lett.*, 2004, **397**, 479–483.
- 86 C. K. Lin, Y. Luo, H. You, Z. W. Quan, J. Zhang, J. Fang and J. Lin, *Chem. Mater.*, 2006, **18**, 458–464.
- 87 C. M. Zhang, H. Z. Lian, D. Y. Kong, S. S. Huang and J. Lin, *J. Phys. Chem. C*, 2009, **113**, 1580–1588.
- 88 C. M. Zhang, C. K. Lin, C. X. Li, Z. W. Quan, X. M. Liu and J. Lin, *J. Phys. Chem. C*, 2008, **112**, 2183–2192.
- 89 C. K. Lin, M. Yu, Z. Y. Cheng, C. M. Zhang, Q. G. Meng and J. Lin, *Inorg. Chem.*, 2008, **47**, 49–55.
- 90 P. P. Yang, P. Yang, X. Teng, J. Lin and L. Huang, *J. Mater. Chem.*, 2011, **21**, 5505–5510.
- 91 P. S. Pizani, E. R. Leite, F. M. Pontes, E. C. Paris, J. H. Rangel, E. J. H. Lee, E. Longo, P. Delega and J. A. Varela, *Appl. Phys. Lett.*, 2000, **77**, 824–826.
- 92 F. M. Pontes, E. R. Leite, E. Longo, J. A. Varela, P. S. Pizani, C. E. M. Campos and F. Lanciotti, *Adv. Mater. Opt. Electron.*, 2000, **10**, 81–89.

- 93 C. Burda, X. B. Chen, R. Narayanan and M. A. El-Sayed, *Chem. Rev.*, 2005, **105**, 1025–1102.
- 94 C. M. Zhang, C. X. Li, C. Peng, R. T. Chai, S. S. Huang, D. M. Yang, Z. Y. Cheng and J. Lin, *Chem.–Eur. J.*, 2010, **16**, 5672–5680.
- 95 J. Yang, C. K. Lin, Z. L. Wang and J. Lin, *Inorg. Chem.*, 2006, **45**, 8973–8979.
- 96 C. X. Li, J. Yang, Z. W. Quan, P. P. Yang, D. Y. Kong and J. Lin, *Chem. Mater.*, 2007, **19**, 4933–4942.
- 97 X. M. Zhang, Z. W. Quan, J. Yang, P. P. Yang, H. Z. Lian and J. Lin, *Nanotechnology*, 2008, **19**, 075603.
- 98 P. A. Tanner and L. X. Yu, *J. Nanosci. Nanotechnol.*, 2008, **8**, 1307–1311.
- 99 Q. A. Ju, W. Q. Luo, Y. S. Liu, H. M. Zhu, R. F. Li and X. Y. Chen, *Nanoscale*, 2010, **2**, 1208–1212.
- 100 Y. D. Yin and A. P. Alivisatos, *Nature*, 2005, **437**, 664–670.
- 101 A. R. Tao, S. Habas and P. D. Yang, *Small*, 2008, **4**, 310–325.
- 102 S. J. Zeng, G. Z. Ren and Q. B. Yang, *J. Mater. Chem.*, 2010, **20**, 2152–2156.
- 103 C. M. Zhang, J. Yang, Z. W. Quan, P. P. Yang, C. X. Li, Z. Y. Hou and J. Lin, *Cryst. Growth Des.*, 2009, **9**, 2725–2733.
- 104 C. M. Zhang, Z. Y. Cheng, P. P. Yang, Z. H. Xu, C. Peng, G. G. Li and J. Lin, *Langmuir*, 2009, **25**, 13591–13598.
- 105 C. M. Zhang, S. S. Huang, D. M. Yang, X. J. Kang, M. M. Shang, C. Peng and J. Lin, *J. Mater. Chem.*, 2010, **20**, 6674–6680.
- 106 C. M. Zhang, C. X. Li, S. S. Huang, Z. Y. Hou, Z. Y. Cheng, P. P. Yang, C. Peng and J. Lin, *Biomaterials*, 2010, **31**, 3374–3383.
- 107 J. J. M. Donners, R. J. M. Nolte and N. A. J. M. Sommerdijk, *Adv. Mater.*, 2003, **15**, 313–316.
- 108 M. H. Cao, C. W. Hu, Y. H. Wang, Y. H. Guo, C. X. Guo and E. B. Wang, *Chem. Commun.*, 2003, 1884–1885.
- 109 M. Johnson, C. F. Richardson, J. D. Sallis and G. H. Nancollas, *Calcif. Tissue Int.*, 1991, **49**, 134–137.
- 110 C. X. Li, Z. H. Xu, D. M. Yang, Z. Y. Cheng, Z. Y. Hou, P. Ma and J. Lin, *CrystEngComm*, 2012, **14**, 670–678.
- 111 A. M. Jakob and T. A. Schmedake, *Chem. Mater.*, 2006, **18**, 3173–3175.
- 112 C. M. Zhang, C. X. Li, J. Yang, Z. Y. Cheng, Z. Y. Hou, Y. Fan and J. Lin, *Langmuir*, 2009, **25**, 7078–7083.
- 113 L. Wang, M. C. Estévez, M. O'Donoghue and W. H. Tan, *Langmuir*, 2008, **24**, 1635–1639.
- 114 D. Y. Kong, C. M. Zhang, Z. H. Xu, G. G. Li, Z. Y. Hou and J. Lin, *J. Colloid Interface Sci.*, 2010, **352**, 278–284.
- 115 X. Xu and X. Wang, *Inorg. Chem.*, 2009, **48**, 3890–3895.
- 116 J. Widoniak, S. Eiden-Assmann and G. Maret, *Eur. J. Inorg. Chem.*, 2005, **2005**, 3149–3155.
- 117 W. Stöber, A. Fink and E. Bohn, *J. Colloid Interface Sci.*, 1968, **26**, 62–69.
- 118 R. P. Bagwe, C. Yang, L. R. Hilliard and W. Tan, *Langmuir*, 2004, **20**, 8336–8342.
- 119 S. Zanarini, E. Rampazzo, L. Della Ciana, M. Marcaccio, E. Marzocchi, M. Montalti, F. Paolucci and L. Prodi, *J. Am. Chem. Soc.*, 2009, **131**, 2260–2267.
- 120 S. Zanarini, E. Rampazzo, S. Bonacchi, R. Juris, M. Marcaccio, M. Montalti, F. Paolucci and L. Prodi, *J. Am. Chem. Soc.*, 2009, **131**, 14208–14209.
- 121 S. Bonacchi, D. Genovese, R. Juris, M. Montalti, L. Prodi, E. Rampazzo and N. Zaccheroni, *Angew. Chem., Int. Ed.*, 2011, **50**, 4056–4066.
- 122 A. Formhals, *US Patent Specification*, 1934, 1975504.
- 123 S. Madhugiri, A. Dalton, J. Gutierrez, J. P. Ferraris and K. J. Balkus, Jr., *J. Am. Chem. Soc.*, 2003, **125**, 14531–14538.
- 124 H. Q. Hou and D. H. Reneker, *Adv. Mater.*, 2004, **16**, 69–73.
- 125 J. J. Ge, H. Hou, Q. Li, M. J. Graham, A. Greiner, D. H. Reneker, F. W. Harris and S. Z. D. Cheng, *J. Am. Chem. Soc.*, 2004, **126**, 15754–15761.
- 126 M. J. Li, J. H. Zhang, H. Zhang, Y. F. Liu, C. L. Wang, X. Xu, Y. Tang and B. Yang, *Adv. Funct. Mater.*, 2007, **17**, 3650–3656.
- 127 Z. Y. Hou, P. P. Yang, H. Z. Lian, L. L. Wang, C. M. Zhang, C. X. Li, R. T. Chai, Z. Y. Cheng and J. Lin, *Chem.–Eur. J.*, 2009, **15**, 6973–6982.
- 128 Z. Y. Hou, G. G. Li, H. Z. Lian and J. Lin, *J. Mater. Chem.*, 2012, **22**, 5254–5276.
- 129 Z. Y. Hou, C. M. Zhang, C. X. Li, Z. H. Xu, Z. Y. Cheng, G. G. Li, W. X. Wang, C. Peng and J. Lin, *Chem.–Eur. J.*, 2010, **16**, 14513–14519.
- 130 G. P. Dong, X. F. Liu, X. D. Xiao, Q. Zhang, G. Lin, Z. J. Ma, D. P. Chen and J. R. Qiu, *Electrochim. Solid-State Lett.*, 2009, **12**, K53–K55.
- 131 C. C. Yu, M. Yu, C. X. Li, C. M. Zhang, P. P. Yang and J. Lin, *Cryst. Growth Des.*, 2009, **9**, 783–791.
- 132 C. X. Li, C. K. Lin, X. M. Liu and J. Lin, *J. Nanosci. Nanotechnol.*, 2008, **8**, 1183–1190.
- 133 K. S. Suslick, S. B. Choe, A. A. Cichowlas and M. W. Grinstaff, *Nature*, 1991, **353**, 414–416.
- 134 T. Iwakasa, K. Inoue, R. Katayama and T. Uchino, *J. Phys. Chem. C*, 2012, **116**, 6754–6761.
- 135 N. A. Dhas, C. P. Raj and A. Gedanken, *Chem. Mater.*, 1998, **10**, 3278–3281.
- 136 M.-L. Terranova, V. Sessa and M. Rossi, *Chem. Vap. Deposition*, 2006, **12**, 315–325.
- 137 J. Hu and R. G. Gordon, *J. Appl. Phys.*, 1992, **71**, 880–890.
- 138 S. Y. Pung, K. L. Choy, X. Hou and K. Dinsdale, *Nanotechnology*, 2010, **21**, 345602.
- 139 R. Salhi, R. Maalej, M. Fourati, Y. Guyot, O. Chaix-Pluchery, L. Rapenne, C. Jimenez and J. L. Deschanvres, *J. Lumin.*, 2011, **131**, 2311–2316.
- 140 L. Gao, W. Ren, H. Xu, L. Jin, Z. Wang, T. Ma, L. P. Ma, Z. Zhang, Q. Fu, L. M. Peng, X. Bao and H. M. Cheng, *Nat. Commun.*, 2012, **3**, 699.
- 141 F. N. Timofeev, A. Aydinli, R. Ellialtioglu, K. Turkoglu, M. Gure, V. N. Mikhailov and O. A. Lavrova, *Solid State Commun.*, 1995, **95**, 443–447.
- 142 N. M. Park, T. S. Kim and S. J. Park, *Appl. Phys. Lett.*, 2001, **78**, 2575–2577.
- 143 E. Neu, M. Fischer, S. Gsell, M. Schreck and C. Becher, *Phys. Rev. B: Condens. Matter Mater. Phys.*, 2011, **84**, 205211.
- 144 N. W. Wang, Y. H. Yang and G. W. Yang, *J. Phys. Chem. C*, 2009, **113**, 15480–15483.
- 145 X. H. An, G. W. Meng, Q. Wei, X. R. Zhang, Y. F. Hao and L. D. Zhang, *Adv. Mater.*, 2005, **17**, 1781–1784.
- 146 H. D. Jang, H. Chang, Y. Suh and K. Okuyama, *Curr. Appl. Phys.*, 2006, **6**, e110–e113.
- 147 J. Liang, Z. Deng, X. Jiang, F. Li and Y. Li, *Inorg. Chem.*, 2002, **41**, 3602–3607.
- 148 J. Jang and H. Yoon, *Adv. Mater.*, 2004, **16**, 799–802.
- 149 J. Zhang and J. Lin, *Microporous Mesoporous Mater.*, 2004, **75**, 115–120.
- 150 Z. Chen, Y. X. Wang, H. P. He, Y. M. Zou, J. W. Wang and Y. Li, *Solid State Commun.*, 2005, **135**, 247–250.
- 151 L. A. Balagurov, B. M. Leifertov, E. A. Petrova, A. F. Orlov and E. M. Panasenko, *J. Appl. Phys.*, 1996, **79**, 7143–7147.
- 152 H. Nishikawa, E. Watanabe and D. Ito, *J. Appl. Phys.*, 1996, **80**, 3513–3517.
- 153 H. Nishikawa, T. Shiroyama, R. Nakamura and Y. Okhi, *Phys. Rev. B: Condens. Matter*, 1992, **45**, 586–591.
- 154 K. Awazu and K. Kawazoe, *J. Appl. Phys.*, 1990, **68**, 3584–3591.
- 155 M. R. Ayers and A. J. Hunt, *J. Non-Cryst. Solids*, 1997, **217**, 229–235.
- 156 B. H. Augustine and E. A. Irene, *J. Appl. Phys.*, 1995, **78**, 4020–4030.
- 157 Y. H. Zhou, J. Lin, X. M. Han, S. B. Wang and H. J. Zhang, *Mater. Res. Bull.*, 2003, **38**, 1289–1299.
- 158 L. S. Wang, Y. H. Zhou, Z. W. Quan and J. Lin, *Mater. Lett.*, 2005, **59**, 1130–1133.
- 159 K. Y. Jung, D. Y. Lee, Y. C. Kang and H. D. Park, *J. Lumin.*, 2003, **105**, 127–133.
- 160 Y. Shimomura and N. Kijima, *J. Electrochem. Soc.*, 2004, **151**, H86–H92.
- 161 A. Vecht, C. Gibbons, D. Davies, X. Jing, P. Marsh, T. G. Ireland, J. Silver, A. Newport and D. Barber, *J. Vac. Sci. Technol. B*, 1999, **17**, 750–757.
- 162 W. Wang, D. L. Shi, J. Lian, Y. Guo, G. K. Liu, L. M. Wang and R. C. Ewing, *Appl. Phys. Lett.*, 2006, **89**, 183106.
- 163 L. Li, Y. Liu, J. Tao, M. Zhang, H. Pan, X. Xu and R. Tang, *J. Phys. Chem. C*, 2008, **112**, 12219–12224.
- 164 H. Tang, Y. S. Liu, W. Q. Luo, R. Li and X. Y. Chen, *J. Nanosci. Nanotechnol.*, 2011, **11**, 9445–9450.
- 165 N. Zhao, D. Pan, W. Nie and X. Ji, *J. Am. Chem. Soc.*, 2006, **128**, 10118–10124.
- 166 Y. Du, W. L. Cai, C. M. Mo, J. Chen, L. D. Zhang and X. G. Zhu, *Appl. Phys. Lett.*, 1999, **74**, 2951–2953.

- 167 J. H. Chen, C. P. Huang, C. G. Chao and T. M. Chen, *Appl. Phys. A: Mater. Sci. Process.*, 2006, **84**, 297–300.
- 168 W. J. Zhang, X. L. Wu, J. Y. Fan, G. S. Huang, T. Qiu and P. K. Chu, *J. Phys.: Condens. Matter*, 2006, **18**, 9937–9942.
- 169 C. W. Raubach, M. Z. Krolow, M. F. Mesko, S. Cava, M. L. Moreira, E. Longo and N. L. V. Carreño, *CrystEngComm*, 2012, **14**, 393–396.
- 170 C. K. Lin, C. M. Zhang and J. Lin, *J. Lumin.*, 2009, **129**, 1469–1474.
- 171 Z. L. Wang, Z. W. Quan and J. Lin, *Inorg. Chem.*, 2007, **46**, 5237–5242.
- 172 J. W. Wang and P. A. Tanner, *J. Am. Chem. Soc.*, 2010, **132**, 947–948.
- 173 K. Ogata, K. Sakurai, S. Fujita, S. Fujita and K. Matsushige, *J. Cryst. Growth*, 2000, **214–215**, 312–315.
- 174 S. Cho, J. Ma, Y. Kim, Y. Sun, G. K. L. Wong and J. B. Ketterson, *Appl. Phys. Lett.*, 1999, **75**, 2761–2763.
- 175 Y. S. Liu, W. Q. Luo, R. F. Li, G. K. Liu, M. R. Antonio and X. Y. Chen, *J. Phys. Chem. C*, 2008, **112**, 686–694.
- 176 Z. L. Wang, C. K. Lin, X. M. Liu, G. Z. Li, Y. Luo, Z. W. Quan, H. P. Xiang and J. Lin, *J. Phys. Chem. B*, 2006, **110**, 9469–9476.
- 177 C. V. Manzano, D. Alegre, O. Caballero-Calero, B. Alén and M. S. Martín-González, *J. Appl. Phys.*, 2011, **110**, 043538.
- 178 S. S. Kurbanov, G. N. Panin, T. W. Kim and T. W. Kang, *J. Lumin.*, 2009, **129**, 1099–1104.
- 179 S. H. Jeong, B. S. Kim and B. T. Lee, *Appl. Phys. Lett.*, 2003, **82**, 2625–2627.
- 180 B. J. Jin, S. Im and S. Y. Lee, *Thin Solid Films*, 2000, **366**, 107–110.
- 181 L. E. Greene, M. Law, J. Goldberger, F. Kim, J. C. Johnson, Y. Zhang, R. J. Saykally and P. Yang, *Angew. Chem., Int. Ed.*, 2003, **42**, 3031–3034.
- 182 Y. W. Heo, D. P. Norton and S. J. Pearton, *J. Appl. Phys.*, 2005, **98**, 073502.
- 183 S. A. Studenikin, N. Golego and M. Cocivera, *J. Appl. Phys.*, 1998, **84**, 2287–2294.
- 184 X. Liu, X. Wu, H. Cao and R. P. H. Chang, *J. Appl. Phys.*, 2004, **95**, 3141–3147.
- 185 M. Wang, E. J. Kim, J. S. Chung, E. W. Shin, S. H. Hahn, K. E. Lee and C. Park, *Phys. Status Solidi A*, 2006, **203**, 2418–2425.
- 186 M. Wang, E. J. Kim and S. H. Hahn, *J. Lumin.*, 2011, **131**, 1428–1433.
- 187 A. Kar, S. Kundu and A. Patra, *J. Phys. Chem. C*, 2011, **115**, 118–124.
- 188 T. Hayakawa, T. Enomoto and M. Nogami, *J. Mater. Res.*, 2002, **17**, 1305–1311.
- 189 J. Kong, H. Zhu, R. Li, W. Luo and X. Y. Chen, *Opt.Lett.*, 2009, **34**, 1873–1875.
- 190 B. Liu, C. W. Cheng, R. Chen, Z. X. Shen, H. J. Fan and H. D. Sun, *J. Phys. Chem. C*, 2010, **114**, 3407–3410.
- 191 F. Gu, S. Fen Wang, M. K. Lü, G. J. Zhou, D. Xu and D. R. Yuan, *J. Phys. Chem. B*, 2004, **108**, 8119–8123.
- 192 S. Sun, G. Meng, G. Zhang, J. P. Masse and L. Zhang, *Chem.–Eur. J.*, 2007, **13**, 9087–9092.
- 193 Q. Xiao, Y. Liu, L. Liu, R. Li, W. Luo and X. Y. Chen, *J. Phys. Chem. C*, 2010, **114**, 9314–9321.
- 194 H. J. Zhou, W. P. Cai and L. D. Zhang, *Appl. Phys. Lett.*, 1999, **75**, 495–497.
- 195 Q. Tang, W. Zhou, W. Zhang, S. Ou, K. Jiang, W. Yu and Y. T. Qian, *Cryst. Growth Des.*, 2005, **5**, 147–150.
- 196 D. Yu, S. H. Yu, S. Zhang, J. Zuo, D. Wang and Y. T. Qian, *Adv. Funct. Mater.*, 2003, **13**, 497–501.
- 197 J. Yang, C. K. Lin, Z. L. Wang and J. Lin, *Inorg. Chem.*, 2006, **45**, 8973–8979.
- 198 Q. Liu, W. Lu, A. Ma, J. Tang, J. Lin and J. Fang, *J. Am. Chem. Soc.*, 2005, **127**, 5276–5277.
- 199 T. Ogi, Y. Kaihatsu, F. Iskandar, W. N. Wang and K. Okuyama, *Adv. Mater.*, 2008, **20**, 3235–3238.
- 200 M. O. Watanabe, S. Itoh, T. Sasaki and K. Mizushima, *Phys. Rev. Lett.*, 1996, **77**, 187–189.
- 201 W. N. Wang, Y. Kaihatsu, F. Iskandar and K. Okuyama, *Mater. Res. Bull.*, 2009, **44**, 2099–2102.
- 202 Y. Kaihatsu, W. N. Wang, F. Iskandar, T. Ogi and K. Okuyama, *J. Electrochem. Soc.*, 2010, **157**, J329–J333.
- 203 Y. Kaihatsu, F. Iskandar, H. Widiyandari, W. N. Wang and K. Okuyama, *Electrochem. Solid-State Lett.*, 2009, **12**, J33–J36.
- 204 X. Liu, S. Ye, Y. Qiao, G. Dong, Q. Zhang and J. Qiu, *Chem. Commun.*, 2009, 4073–4075.
- 205 X. Liu, Y. Qiao, G. Dong, S. Ye, B. Zhu, Y. Zhuang and J. Qiu, *J. Electrochem. Soc.*, 2009, **156**, P81–P84.
- 206 X. Liu, S. Ye, G. Dong, Y. Qiao, J. Ruan, Y. Zhuang, Q. Zhang, G. Lin, D. Chen and J. Qiu, *J. Phys. D: Appl. Phys.*, 2009, **42**, 215409.
- 207 T. Matsuzawa, Y. Aoki, N. Takeuchi and Y. Murayama, *J. Electrochem. Soc.*, 1996, **143**, 2670–2673.
- 208 W. S. Chao, E. Hamada and K. Takayanagi, *J. Appl. Phys.*, 1997, **81**, 3000–3002.
- 209 A. G. Cullis, L. T. Canhan and P. D. J. Calcott, *J. Appl. Phys.*, 1997, **82**, 909–965.
- 210 D. Yu, Q. Liu and Q. F. Liu, *Acta Phys.-Chim. Sin.*, 2008, **24**, 695–699.
- 211 E. A. V. Ferri, J. C. Sczancoski, L. S. Cavalcante, E. C. Paris, J. W. M. Espinosa, A. T. de Figueiredo, P. S. Pizani, V. R. Mastelaro, J. A. Varela and E. Longo, *Mater. Chem. Phys.*, 2009, **117**, 192–198.
- 212 S. de Lázaro, J. Milanez, A. T. de Figueiredo, V. M. Longo, V. R. Mastelaro, F. S. De Vicente, A. C. Hernandes, J. A. Varela and E. Longo, *Appl. Phys. Lett.*, 2007, **90**, 111904.
- 213 F. M. Pontes, C. D. Pinheiro, E. Longo, E. R. Leite, S. R. de Lázaro, J. A. Varela, P. S. Pizani, T. M. Boschi and F. Lanciotti, *Mater. Chem. Phys.*, 2002, **78**, 227–233.
- 214 Y. Takahashi, K. Kitamura, N. Iyi and S. Inoue, *Appl. Phys. Lett.*, 2006, **88**, 151903.
- 215 W. F. Zhang, X. T. Zhang, Z. Yin, M. S. Zhang, G. H. Ma and Z. L. Du, *Chin. Phys. Lett.*, 1998, **15**, 758–760.
- 216 T. Jüstel, H. Nikol and C. Ronda, *Angew. Chem., Int. Ed.*, 1998, **37**, 3084–3103.
- 217 Y. P. Sun, B. Zhou, Y. Lin, W. Wang, K. A. S. Fernando, P. Pathak, M. J. Meziani, B. A. Harruff, X. Wang, H. F. Wang, P. J. G. Luo, H. Yang, M. E. Kose, B. L. Chen, L. M. Veca and S. Y. Xie, *J. Am. Chem. Soc.*, 2006, **128**, 7756–7757.
- 218 J. G. Zhou, C. Booker, R. Y. Li, X. T. Zhou, T. K. Sham, X. L. Sun and Z. F. Ding, *J. Am. Chem. Soc.*, 2007, **129**, 744–745.
- 219 S. L. Hu, K. Y. Niu, J. Sun, J. Yang, N. Q. Zhao and X. W. Du, *J. Mater. Chem.*, 2009, **19**, 484–488.
- 220 A. B. Bourlinos, A. Stassinopoulos, D. Anglos, R. Zboril, V. Georgakilas and E. P. Giannelis, *Chem. Mater.*, 2008, **20**, 4539–4541.
- 221 R. L. Liu, D. Q. Wu, S. H. Liu, K. Koynov, W. Knoll and Q. Li, *Angew. Chem.*, 2009, **121**, 4668–4671 (*Angew. Chem., Int. Ed.*, 2009, **48**, 4598–4601).
- 222 H. Zhu, X. L. Wang, Y. L. Li, Z. J. Wang, F. Yang and X. R. Yang, *Chem. Commun.*, 2009, 5118–5120.
- 223 A. B. Bourlinos, A. Stassinopoulos, D. Anglos, R. Zboril, M. Karakassides and E. P. Giannelis, *Small*, 2008, **4**, 455–458.
- 224 S. C. Ray, A. Saha, N. R. Jana and R. Sarkar, *J. Phys. Chem. C*, 2009, **113**, 18546–18551.
- 225 L. Tian, D. Ghosh, W. Chen, S. Pradhan, X. Chang and S. Chen, *Chem. Mater.*, 2009, **21**, 2803–2809.
- 226 Q. L. Zhao, Z. L. Zhang, B. H. Huang, J. Peng, M. Zhang and D. W. Pang, *Chem. Commun.*, 2008, 5116–5118.
- 227 H. P. Liu, T. Ye and C. D. Mao, *Angew. Chem.*, 2007, **119**, 6593–6595 (*Angew. Chem., Int. Ed.*, 2007, **46**, 6473–6475).
- 228 S. T. Yang, X. Wang, H. Wang, F. Lu, P. G. Luo, L. Cao, M. J. Meziani, J. H. Liu, Y. Liu, M. Chen, Y. Huang and Y. P. Sun, *J. Phys. Chem. C*, 2009, **113**, 18110–18114.
- 229 X. Sun, Z. Liu, K. Welsher, J. T. Robinson, A. Goodwin, S. Zaric and H. J. Dai, *Nano Res.*, 2008, **1**, 203–212.
- 230 Z. Liu, J. T. Robinson, X. Sun and H. J. Dai, *J. Am. Chem. Soc.*, 2008, **130**, 10876–10877.
- 231 Z. T. Luo, P. M. Vora, E. J. Mele, A. T. C. Johnson and J. M. Kikkawa, *Appl. Phys. Lett.*, 2009, **94**, 111909.
- 232 T. Gokus, R. R. Nair, A. Bonetti, M. Bohmller, A. Lombardo, K. S. Novoselov, A. K. Geim, A. C. Ferrari and A. Hartschuh, *ACS Nano*, 2009, **3**, 3963–3968.
- 233 D. Pan, J. Zhang, Z. Li and M. Wu, *Adv. Mater.*, 2010, **22**, 734–738.
- 234 J. Shen, Y. Zhu, C. Chen, X. Yang and C. Li, *Chem. Commun.*, 2011, **47**, 2580–2582.

- 235 G. Eda, Y. Y. Lin, C. Mattevi, H. Yamaguchi, H. A. Chen, I. S. Chen, C. W. Chen and M. Chhowalla, *Adv. Mater.*, 2010, **22**, 505–509.
- 236 H. Li, S. Inoue, D. Ueda, K. Machida and G. Adachi, *Electrochem. Solid-State Lett.*, 1999, **2**, 354–356.
- 237 M. Falossi, M. Canva, P. Georges, A. Brun, F. Chaput and J. P. Boilot, *Appl. Opt.*, 1997, **36**, 6760–6763.
- 238 D. Blanc, S. Pelissier, K. Saravanamuttu, S. I. Najafi and M. P. Andrews, *Adv. Mater.*, 1999, **11**, 1508–1511.
- 239 S. S. Nobre, P. P. Lima, L. Mafra, R. A. S. Ferreira, R. O. Freire, L. S. Fu, U. Pischel, V. D. Bermudez, O. L. Malta and L. D. Carlos, *J. Phys. Chem. C*, 2007, **111**, 3275–3284.
- 240 L. D. Carlos, R. A. S. Ferreira, V. D. Bermudez and S. J. L. Ribeiro, *Adv. Funct. Mater.*, 2001, **11**, 111–115.
- 241 M. S. Wang, G. C. Guo, W. T. Chen, G. Xu, W. W. Zhou, K. J. Wu and J. S. Huang, *Angew. Chem., Int. Ed.*, 2007, **46**, 3909–3911.
- 242 S. Ye, F. Xiao, Y. X. Pan, Y. Y. Ma and Q. Y. Zhang, *Mater. Sci. Eng., R*, 2010, **71**, 1–34.
- 243 C. C. Lin, Z. R. Xiao, G. Y. Guo, T. S. Chan and R. S. Liu, *J. Am. Chem. Soc.*, 2010, **132**, 3020–3028.
- 244 K. S. Sohn, D. H. Park, S. H. Cho, J. S. Kwak and J. S. Kim, *Chem. Mater.*, 2006, **18**, 1768–1772.
- 245 L. Chen, C. C. Lin, C. W. Yeh and R. S. Liu, *Materials*, 2010, **3**, 2172–2195.
- 246 C. C. Lin, R. S. Liu, Y. S. Tang and S. F. Hu, *J. Electrochem. Soc.*, 2008, **155**, J248–J251.
- 247 S. C. Huang, J. K. Wu, W. J. Hsu, H. H. Chang, H. Y. Hung, C. L. Lin, H. Y. Su, N. Bagkar, W. C. Ke, H. T. Kuo and R. S. Liu, *Int. J. Appl. Ceram. Technol.*, 2009, **6**, 465–469.
- 248 M. S. Wang, S. P. Guo, Y. Li, L. Z. Cai, J. P. Zou, G. Xu, W. W. Zhou, F. K. Zheng and G. C. Guo, *J. Am. Chem. Soc.*, 2009, **131**, 13572–13573.
- 249 L. P. Li, Y. G. Su and G. G. Li, *J. Mater. Chem.*, 2010, **20**, 459–465.
- 250 F. Liu, L. D. Carlos, R. A. S. Ferreira, J. Rocha, M. C. Gaudino, M. Robitzer and F. Quignard, *Biomacromolecules*, 2008, **9**, 1945–1950.
- 251 C. Kulshreshtha, J. H. Kwak, Y. J. Park and K. S. Sohn, *Opt. Lett.*, 2009, **34**, 794–796.
- 252 A. Zumbuehl, D. Jeannerat, S. E. Martin, M. Sohrmann, P. Stano, T. Vigassy, D. D. Clark, S. L. Hussey, M. Peter, B. R. Peterson, E. Pretsch, P. Walde and E. M. Carreira, *Angew. Chem., Int. Ed.*, 2004, **43**, 5181–5185.
- 253 K. T. Yong, H. Ding, I. Roy, W. C. Law, E. J. Bergey, A. Maitra and P. N. Prasad, *ACS Nano*, 2009, **3**, 502–510.
- 254 K. E. Uhrich, S. M. Cannizzaro, R. S. Langer and K. M. Shakesheff, *Chem. Rev.*, 1999, **99**, 3181–3198.
- 255 J. L. Vivero-Escoto, I. I. Slowing, C. W. Wu and V. S. Y. Lin, *J. Am. Chem. Soc.*, 2009, **131**, 3462–3463.
- 256 F. H. Chen, Q. Gao and J. Z. Ni, *Nanotechnology*, 2008, **19**, 165103.
- 257 J. Ritter, A. Ebner, K. Daniel and K. Stewart, *J. Magn. Magn. Mater.*, 2004, **280**, 184–201.
- 258 P. P. Yang, S. S. Huang, D. Y. Kong, J. Lin and H. Q. Fu, *Inorg. Chem.*, 2007, **46**, 3203–3211.
- 259 M. Vallet-Regi, A. Rámila, R. P. Del-Real and J. A. Pérez-Priente, *Chem. Mater.*, 2001, **13**, 308–311.
- 260 Z. Li, J. C. Barnes, A. Bosoy, J. F. Stoddart and J. I. Zink, *Chem. Soc. Rev.*, 2012, **41**, 2590–2605.
- 261 L. Zhao, T. Ming, H. Chen, L. Gong, J. Chen and J. Wang, *Phys. Chem. Chem. Phys.*, 2011, **13**, 2387–2393.
- 262 Q. He, J. Shi, X. i Cui, C. Wei, L. Zhang, W. Wu, W. Bu, H. Chen and H. Wu, *Chem. Commun.*, 2011, **47**, 7947–7949.
- 263 X. H. Gao, L. L. Yang, J. A. Petros, F. F. Marshal, J. W. Simons and S. M. Nie, *Curr. Opin. Biotechnol.*, 2005, **16**, 63–72.
- 264 R. Hardman, *Environ. Health Perspect.*, 2006, **114**, 165–172.
- 265 J. K. Jaiswal and S. M. Simon, *Trends Cell Biol.*, 2004, **14**, 497–504.
- 266 Y. I. Park, J. H. Kim, K. T. Lee, K. S. Jeon, H. B. Na, J. H. Yu, H. M. Kim, N. Lee, S. H. Choi, S. I. Baik, H. Kim, S. P. Park, B. J. Park, Y. W. Kim, S. H. Lee, S. Y. Yoon, I. C. Song, W. K. Moon, Y. D. Suh and T. Hyeon, *Adv. Mater.*, 2009, **21**, 4467–4471.
- 267 C. X. Li and J. Lin, *J. Mater. Chem.*, 2010, **20**, 6831–6847.
- 268 L. Cao, X. Wang, M. J. Meziani, F. S. Lu, H. F. Wang, P. J. G. Luo, Y. Lin, B. A. Harruff, L. M. Veca, D. Murray, S. Y. Xie and Y. P. Sun, *J. Am. Chem. Soc.*, 2007, **129**, 11318–11319.
- 269 S. T. Yang, L. Cao, P. G. Luo, F. S. Lu, X. Wang, H. F. Wang, M. J. Meziani, Y. F. Liu, G. Qi and Y. P. Sun, *J. Am. Chem. Soc.*, 2009, **131**, 11308–11309.